Oscillatory calcium release and sustained store-operated oscillatory calcium signaling prevents differentiation of human oligodendrocyte progenitor cells

Richard A. Seidman[1], Heba Khattab[2], Jessie J. Polanco[1], Jacqueline E. Broome[2], Fraser J. Sim[1,2]

Neuroscience Program[1], Department of Pharmacology and Toxicology[2], Jacobs School of Medicine and Biomedical Sciences, University at Buffalo, Buffalo, NY.

Address correspondence to:
Fraser Sim, Ph.D.
Department of Pharmacology and Toxicology
Jacob's School of Medicine and Biomedical Sciences
University at Buffalo
955 Main Street
Buffalo, NY 14203
716-829-2151
fjsim@buffalo.edu

Keywords: human, lentivirus, STIM1, STIM2, muscarinic receptor, metabotropic glutamate receptor
Running title: STIM-dependent Ca-signaling blocks hOPC differentiation.

Abstract, 242 words; Introduction, 862 words; Discussion, 1753 words.
Figures: 5; Tables: 2

Acknowledgements:

This work was supported by grants from the NINDS (R01NS104021), the National Multiple Sclerosis Society (RG 5505-A-2, RG 5110A1/1), the Kalec Multiple Sclerosis Foundation, the Change MS Foundation, and the Skarlow Memorial Trust. JJP received support from NIGMS (R25GM09545902), NCATS (UL1TR001412-S1). JJP and RAS received support from NYSTEM Stem Cells in Regenerative Medicine Fellowship (#C302090G). In addition, we would like to acknowledge the assistance of the Confocal Microscope and Flow Cytometry Facility in the School of Medicine and Biomedical Sciences, University at Buffalo and thank Dr. Pablo Paez for advice with calcium imaging of OPCs.

ABSTRACT

Endogenous remyelination in demyelinating diseases such as multiple sclerosis is contingent upon the successful differentiation of oligodendrocyte progenitor cells (OPCs). Signaling via the $G\alpha_q$-coupled muscarinic receptor ($M_{1/3}R$) inhibits human OPC differentiation and impairs endogenous remyelination in experimental models. We hypothesized that calcium release following $G\alpha_q$-coupled receptor (G_qR) activation directly regulates human OPC (hOPC) cell fate. In this study, we show that specific G_qR agonists activating muscarinic and metabotropic glutamate receptors induce characteristic oscillatory calcium release in hOPCs and that these agonists similarly block hOPC maturation *in vitro*. Both agonists induce calcium release from endoplasmic reticulum (ER) stores and store operated calcium entry (SOCE) likely via STIM/ORAI-based channels. siRNA mediated knockdown (KD) of obligate calcium sensors STIM1 and STIM2 decreased the magnitude of muscarinic agonist induced oscillatory calcium release and attenuated SOCE in hOPCs. In addition, STIM2 expression was necessary to maintain the frequency of calcium oscillations and STIM2 KD reduced spontaneous OPC differentiation. Furthermore, STIM2 siRNA prevented the effects of muscarinic agonist treatment on OPC differentiation suggesting that SOCE is necessary for the anti-differentiative action of muscarinic receptor-dependent signaling. Finally, using a gain-of-function approach with an optogenetic STIM lentivirus, we demonstrate that independent activation of SOCE was sufficient to significantly block hOPC differentiation and this occurred in a frequency dependent manner while increasing hOPC proliferation. These findings suggest that intracellular calcium oscillations directly regulate hOPC fate and that modulation of calcium oscillation frequency may overcome inhibitory $G\alpha_q$-coupled signaling that impairs myelin repair.

Significance Statement

In this study, Seidman et al. show that SOCE is a common component of ligand-based $G\alpha_q$-coupled signaling in hOPCs and that SOCE alone is sufficient to block hOPC differentiation and drive proliferation. Therefore, SOCE blocks differentiation and pathological SOCE could contribute to myelin disease.

60 **INTRODUCTION**

61 Efficient central nervous system (CNS) remyelination is contingent upon successful intercellular
62 signaling between neurons and glia that together orchestrate the processes of oligodendrocyte progenitor
63 cell (OPC) recruitment, differentiation, and maturation into myelin-forming oligodendrocytes (OL) [1]. In
64 demyelinating diseases such as multiple sclerosis (MS), the pathological environment contributes to an
65 inhibition of OPC differentiation that limits remyelination and may contribute to subsequent permanent
66 neurodegeneration [2]. In support of this hypothesis, numerous quiescent OPCs are observed in chronic
67 MS lesions that appear to be unable to undergo OL differentiation [3,4]. Following demyelination, OPCs are
68 exposed to a complex cellular microenvironment comprising extracellular matrix and soluble factors
69 released by a variety of sources including infiltrating immune cells, reactive glia, and endothelial cells as
70 well as injured axons that release both soluble growth factors and neurotransmitters. Neurotransmitters
71 activate multiple and functionally distinct receptors expressed on OPCs and OLs that may contribute to
72 activity-dependent or so-called adaptive myelination (reviewed in [5]). Following demyelination, neuronal
73 activity promotes remyelination [6] and this is regulated in part by AMPA and NMDA receptor signaling [7].
74 As such, intracellular calcium represents a common target for these activity-dependent pathways and
75 suggests that a diverse set of neurotransmitters can induce intracellular calcium increase in glial
76 progenitors [8].

77 Intracellular calcium release occurs in OPCs following activation of ionotropic voltage and ligand
78 gated channels and/or following activation of metabotropic receptors [9]. Muscarinic acetylcholine
79 receptors M_1 and M_3 are $G\alpha_q$-coupled receptors (G_qR) which also cause intracellular calcium release via
80 phospholipase-Cβ (PLCβ) and inositol trisphosphate (IP_3) second messengers [10]. Genetic deletion of $M_{1/3}$
81 receptors in OPCs delays differentiation and remyelination in animal models of experimental
82 demyelination [11,12]. Furthermore, pharmacological inhibition of muscarinic receptors results in accelerated
83 OL differentiation and remyelination in the brain and spinal cord following both toxin-induced
84 demyelination and experimental autoimmune encephalitis (EAE) [11,13-15]. In primary human OPCs
85 (hOPCs), $M_{1/3}R$ signaling delays differentiation *in vitro* and reduces myelin production following
86 transplantation into hypomyelinated *shiverer* mice [12]. OPCs have been shown to express numerous other
87 $G\alpha_q$-coupled receptors including endothelin (ET) subtype B (ET_B; ENDRB) receptors [16], purinergic type
88 2Y (P2Y) receptors [17], histamine type 1 (H1) receptors [18], metabotropic glutamate receptors type 3
89 ($mGluR_3$) and type 5 ($mGluR_5$) [19], 5-HT serotonin receptors [20], sphingosine-1-phosphate receptors
90 (S1PR) [21], calcium-sensing receptors (CaSR) [22], and adenosine 2B receptors [23]. While the precise
91 function of these receptors remains unclear, previous reports suggest that activation of at least some of
92 these receptors can paradoxically promote OPC differentiation. For example, *in vitro* findings suggest
93 that ET receptor agonists increase OPC migration and block proliferation [16]. Stimulation of myelin basic

94 protein (MBP) expression occurs via ET_A [24] receptor activity, and activation of ET_B receptors has been
95 found to promote remyelination in cerebellar slice culture [25]. Likewise, conditional deletion of S1PR
96 causes increased OPC proliferation and reduced oligodendrocyte differentiation [26], while CaSR null mice
97 exhibit reduced MBP expression during development [22]. Despite these findings, the key signaling
98 components downstream of muscarinic receptor activation that act to delay OPC differentiation and
99 distinguish $M_{1/3}R$ from other $G\alpha_q$-receptors have not yet been established.

100 Following activation of $G\alpha_q$-coupled receptors and calcium release from the endoplasmic
101 reticulum (ER), calcium sensing STIM proteins in the ER membrane oligomerize and complex with ORAI
102 channel proteins located in the plasma membrane. These calcium release activated calcium (CRAC)
103 channels mediate store operated calcium entry (SOCE) that replenish depleted ER-stores through
104 sarcoplasmic/endoplasmic reticulum ATPase (SERCA) pumps [27]. Successive activation of ER-calcium
105 release and CRAC channel influx events result in characteristic oscillatory calcium transients [28].
106 Intriguingly, the frequency encoding of oscillatory calcium signaling is associated with cell-type specific
107 activation of distinct downstream signaling and gene expression [28,29]. In rodent OPCs, *in vitro* application
108 of a pharmacological SOCE antagonist limits platelet derived growth factor (PDGF)-dependent
109 proliferation [30]. However, the mechanisms of action of these drugs are complex with additional actions
110 on IP_3 receptors, gap junction permeability, and transient receptor potential channels. Furthermore, while
111 ligand-induced calcium oscillations have been observed in OL lineage cells [19,31,32], a specific role of
112 calcium oscillations in human OPCs has not yet been determined.

113 In this study, we hypothesized that the specific oscillatory signature of ligand activated $G\alpha_q$-
114 receptor mediated calcium responses may be responsible for the regulation of hOPC differentiation. To
115 this end, we identified several $G\alpha_q$-coupled receptors expressed by hOPCs and characterized the calcium
116 response following application of receptor subtype-specific ligands. Only activation of muscarinic
117 acetylcholine $M_{1/3}$ receptors or metabotropic type 5 glutamate receptors ($mGluR_5$) resulted in oscillatory
118 transients in a large fraction of OPCs and persisted for several minutes following application of the ligand.
119 Intriguingly, these ligands also reduced hOPC differentiation. We demonstrate that SOCE downstream
120 of $M_{1/3}R$ ligand activation is dependent on ER calcium sensors STIM1/2. More specifically, we found that
121 both STIM proteins contribute to the magnitude of SOCE in human OPCs and that STIM2 regulates the
122 oscillatory frequency of $M_{1/3}R$-induced calcium responses. Knockdown of STIM2 resulted in reduced OL
123 differentiation and prevented the anti-differentiative effects of $M_{1/3}R$ signaling in hOPCs. Lastly, using
124 optogenetic activation of CRAC-mediated calcium flux, we demonstrate that SOCE induction is sufficient
125 to inhibit hOPC differentiation in the absence of G_qR signaling and that modulation of OPC proliferation
126 and differentiation was dependent on SOCE frequency.

127 **MATERIALS AND METHODS**

128 *Human CD140a/PDGFαR cell preparation and culture with $G\alpha_q$-agonists*

129 Fetal brain tissue samples, between 17 and 22 weeks of gestational age, were obtained from
130 Advanced Bioscience Resources (Alameda, CA) with informed consent obtained from all donors. All
131 research was performed in accordance with relevant guidelines/regulations. Following review by the
132 University at Buffalo Research Subjects Institutional Review Board the tissue acquisition and research
133 was not deemed to involve human subjects as defined under HHS regulations 45 CFR 46, 102 (f).
134 Forebrain samples were minced and dissociated using papain and DNase as previously described [33].
135 Magnetic sorting of CD140a/PDGFαR positive cells was performed as described [34].

136 *Plasmid construction, lentiviral generation, and titration*

137 EF1α:GCaMP6s was described previously [12]. EF1α:jRCaMP1a was cloned as follows. pGP-CMV-
138 NES-jRCaMP1a was obtained from AddGene (#61562) [35]. The nuclear export signal (NES) and
139 jRCaMP1a coding region was PCR amplified: SpeI, forward–5'
140 AAAACTAGTGAACCGTCAGATCCGCTAG-3';PspXI (Thermo Fisher Scientific), reverse, 5'-
141 AAAGCTCGAGCTCTACAAATGTGGTATGGCTG-3' (Thermo Fisher Scientific). PCR products were
142 purified (Monarch PCR Cleanup Kit (NEB, #T1030S)) and restriction digested with unique 5' SpeI and 3'
143 PspXI sites, and purified again. NES-jRCaMP1a digested PCR fragments were then ligated into lentiviral
144 pTRIP-EF1α vector (a gift of Abdel Benraiss, University of Rochester)[36]. The plasmid pLenti-EF1α-
145 OptoSTIM was a gift from Taeyoon Kyung (KAIST, DAEJEON, Republic of Korea) [37]. Lentiviruses were
146 generated as described [38] and titration of EF1α:GCaMP6s and EF1α:OptoSTIM was performed as
147 previously described [39]. Optimized multiplicity of infection (MOI) in hOPCs was determined for
148 EF1α:GCaMP6s and EF1α:jRCaMP1a by infecting hOPCs and quantifying proportion of responsive cells
149 following administration of 25μM Oxo-M. Optimal MOI for EF1α:OptoSTIM lentivirus was determined
150 through analysis of optimal GFP expression in infected hOPCs.

151 *Calcium imaging using LV EF1a:GCaMP6s*

152 Calcium imaging was performed as described previously [12]. GCaMP6s infected hOPCs were
153 seeded at 4-5 x 10^4 cells/mL and imaged 24 hours after seeding. All experimental data were generated
154 from independent experiments using individual naïve cultures of hOPCs from separate patient fetal
155 samples. To avoid possible confounds relating to sequential application of small molecules, all cultures
156 were used only once for imaging calcium responses and only a single dose was tested in each well, with
157 two technical replicate imaging fields imaged simultaneous per well for each dose or condition tested. In
158 dose response experiments, all doses per each drug were tested on the same experimental day for each
159 fetal sample preparation. Bright field and fluorescence images were acquired (10x; Olympus IX51

160 microscope with a Exfo X-Cite or Xylis illumination and Hamamatsu ORCA-FLASHv4 camera) using
161 μManager [40]. All drugs were reconstituted and aliquoted within 1-2 weeks and thawed immediately prior
162 to use. Region of interest (ROI) generation and image processing were performed using ImageJ, and
163 analysis of calcium transients was performed in R as described [12].
164 Briefly, per cell calcium responses (raw pixel intensity) were normalized to baseline fluorescence
165 calculated prior to addition of $G\alpha_q$-receptor ligand (F_0, average 5-10 frames). To define calcium peaks
166 and characterize the properties of ligand-induced calcium oscillations, individual cell traces were loess
167 smoothed prior to the identification of local minima and maxima in 16 second windows. Calcium peaks
168 were defined as maxima whose amplitude increased ≥0.35 fold-change above the preceding local
169 minima. Peak amplitude was defined as the difference in fluorescence values from the calcium peak to
170 the preceding local minima. The number of oscillations was defined as the number of peaks identified
171 during the recording session. A responsive cell was defined as any cell with at least one peak, and an
172 oscillatory cell as any cell with two or more peaks. Response duration was measured from the local
173 minima prior to the first peak oscillation to the local minima following the last peak oscillation, or to the
174 end of the time-lapse recording if an on-going calcium peak had not yet reached baseline. For oscillatory
175 cells, frequency was calculated by dividing the total number of peak oscillations by the response duration.
176 Area under the curve (AUC) was calculated (*Mess* package, v0.5.6; https://cran.r-
177 project.org/web/packages/MESS/index.html) by subtraction of F_0, and then analyzed as integral pixel
178 intensity above baseline beginning from the local minima preceding the first identified peak on the
179 normalized calcium curve following ligand stimulation for the duration of the imaged response.
180 Raw data measurements of individual cell calcium responses were assessed for normality. Per-
181 cell AUC and frequency measurements exhibit significant skew and were log-transformed to achieve a
182 near normal distribution. Unless otherwise stated, a linear model was used for one-way ANOVA using
183 drug dose as a covariate, as well as human sample to consider individual sample variability. Non-linear
184 regression was performed using GraphPad Prism (8.0e) using a variable slope-four parameter logistic
185 equation to model and calculate EC_{50} for each drug. For STIM KD experiments, GCaMP6s cells were
186 transfected with STIM siRNA and imaged 24-48h post transfection.

187 *Assessment of store-operated calcium entry*

188 For direct assessment of SOCE, hOPCs were infected with LV-GCaMP6s (1 MOI) and 5 x 10^4
189 cells/mL were seeding in 48-well plates and imaged the following day. To remove extracellular calcium,
190 15 minutes prior to imaging media was replaced with HBSS without phenol red, calcium, and magnesium
191 (Corning, #21-022) (HBSS-). For all conditions, fields were imaged with a 5 second interval for at least
192 15 minutes (488nm excitation, 400ms exposure). Addition of the SERCA blocker Thapsigargin (Tg) or

193 the muscarinic agonist Oxotremorine-Methiodide (Oxo-M) with or without store operated calcium entry
194 (SOCE) channel antagonists occurred at ~1-2 minutes after the start of imaging. Calcium [1.2mM]) was
195 re-introduced 10-15 minutes following addition of Tg or Oxo-M. Final concentrations of compounds were
196 Tg [10μM] or Oxo-M [25μM], and 2-APB [50μM] or MRS-1845 [10μM] (final DMSO concentration did not
197 exceed 0.15%, which did not influence $[Ca^{2+}]_i$). For quantification of SOCE, per cell calcium response
198 curves were normalized to baseline fluorescence F_0 (average of 5-10 frames prior to addition of Oxo-M
199 or Tg). Normalized traces were loess smoothed to identify responsive cells exhibiting ≥0.35 fold increase
200 in GCaMP6s fluorescence from baseline following initial Oxo-M or Tg ER-store depletion. Area under the
201 curve (AUC) was measured for ER depletion for 10 minutes following Oxo-M or Tg ER-store depletion,
202 and AUC for SOCE was measured for 5-8 minutes (**Fig. 1H**) or 8 minutes (**Fig. 2E**) following calcium re-
203 addition. AUC durations were matched between conditions and were quantified. For analysis of SOCE
204 following STIM KO, AUC of SOCE was normalized to the ER-release of control cells in matched biological
205 replicates and quantified using repeated measures (RM) one-way ANOVA with Holm-Sidak's post-hoc
206 test. Maximum amplitude of ER depletion was identified as the maximal peak response >0.35 fold-change
207 increase from baseline following Oxo-M or Tg addition and following calcium re-addition respectively.
208 Cells which did not exhibit an initial ER-store depletion response (≥0.35 fold-change from baseline
209 following Tg or Oxo-M addition and prior to calcium re-addition) were excluded from further analyses.

210 *siRNA transfection*

211 hOPCs were seeded at 5 x 10^4 cells/mL and Lipofectamine RNAi max (Invitrogen, #13778-150)
212 was used to transfect cells according to the manufacturer's protocol with minor alterations. Briefly, stealth
213 RNAi negative control duplex medium GC content (Invitrogen, #12935300) or three combined stealth
214 RNAis against STIM1 (Invitrogen, ID#'s: HSS110308, HSS110309, HSS186144) and/or STIM2
215 (Invitrogen, ID#'s: HSS183972, HSS183973, HSS183974) were pooled and used for transfection. Stealth
216 RNAi (100 nM total RNAi per well) was used to transfect hOPCs per each condition with 1.5% v/v
217 Lipofectamine. For calcium imaging, cells were plated in 48-well plates and imaged 24 hours post-
218 transfection. In differentiation experiments, mitogen containing media was removed 24 hours post-
219 transfection (experimental day 0) and replaced with media without mitogens. Oxo-M [25μM] was added
220 on experimental day 0 upon removal of growth factors and on experimental day 2 during a half media
221 change. hOPCs were fixed on experimental day 3-4 following live staining with mouse x O4 Hybridoma
222 primary antibody [1:25]. Immuno-cytochemical analysis was performed as described previously [33]. For
223 analysis of STIM expression, cells were plated at 5 x 10^4 cells/mL 6-well plates and transfected after 24
224 hours. RNA was extracted 24-48 hours post-transfection for cDNA synthesis and quantitative RT-PCR
225 analysis.

226 *Quantitative RT-PCR analyses*

227 Total RNA was extracted (Omega Biotek) and cDNA was synthesized using SuperScript III
228 reverse transcriptase (Invitrogen, Carlsbad, CA). Human-specific primers for SYBR green-based PCR
229 were designed (**Table 1**). Samples were run in triplicate and gene expression calculated by $\Delta\Delta C_t$ method
230 using GAPDH as a reference. Statistical significance was tested on log_2-transformed data normalized to
231 control using a one-sample t-test assuming equal SD and compared to a hypothetical value of 100
232 (GraphPad Prism 8.0e).

233 *Assessment of long-term OptoSTIM-induced SOCE*

234 For all long-term experiments, hOPCs were seeded at a density of 2.5-3.0 x 10^5 cells/mL into
235 poly-ornithine and laminin coated ibidi tissue culture treated µ-slide VI 0.4 (iBIDI, #80606) in mitogen
236 containing Livelight ND media to reduce phototoxicity [41]. Cells were then imaged in an on-stage ibidi
237 environmentally controlled chamber to maintain 37ºC, 5.0% CO2, and >60% humidity for the duration of
238 each imaging experiment. In long-term calcium imaging experiments, hOPCs were infected with
239 jRCaMP1a (1 MOI) and OptoSTIM (1 MOI) lentiviruses. Two fields per each of 3 µ-slide channels were
240 then imaged at 10x with 594 nm excitation every 20 seconds for 3 hours to measure jRCaMP1a
241 fluorescence calcium responses. After a 30-minute no-stimulation period and for the remainder of
242 imaging, hOPCs were stimulated with 488 nm excitation (every 5 or 30 minutes with 330 and 2000 ms
243 illumination times respectively) to induce SOCE calcium responses. A custom beanshell script was
244 designed and implemented to facilitate multi-channel and multi-position imaging and provide an interface
245 between the motorized stage, fluorescent shutter (Prior), and µManager software. The complete imaging
246 script is available upon request. Analysis of OptoSTIM-induced calcium responses was conducted by
247 implementing the automated tracking plugin TrackMate in ImageJ [42]. Mean fluorescence intensity data
248 within the region of interest for all cells tracked across all frames was exported and subsequently
249 analyzed in R. Briefly, a baseline curve was generated by fitting minima points under each calcium trace
250 using the “spc-Rubberband" function (*hyperSpec* package). Traces were first normalized by division of
251 the baseline curve and loess fitted to identify responsive cells with ≥12.5% increase in jRCaMP1a
252 fluorescence within 2 minutes following the first OptoSTIM 488nm pulse. For quantification of AUC, each
253 tracked cell’s mean jRCaMP1a fluorescence values per each time-point were normalized by subtraction
254 of the baseline curve and AUC was calculated for the duration of the stimulation period. Calcium traces
255 are presented as fold change in jRCaMP1a fluorescence from baseline, averaged across all cells per
256 each time-point with SEM calculated. In differentiation and proliferation experiments, OptoSTIM infected
257 hOPCs (1 MOI) were seeded into µ-slides and bright field imaged for 2–3 days. Following a 10-12 hour
258 baseline period, OptoSTIM activation was initiated with 488nm stimulation at different frequencies (every

259 5 or 30m with 330 or 2000ms illumination times respectively) for the remainder of imaging. After imaging,
260 cells were immunostained for O4 and the number of $O4^+$ and GFP^+ cells were counted and analyzed.
261 Repeated measures (RM) one-way ANOVA was employed with Holm-Sidak's post-hoc test for
262 quantification of the proportion of $O4^+$ to GFP^+ cells and quantification of morphological branching. In
263 proliferation experiments, cell density was counted at the onset of blue light stimulation and mitotic events
264 were identified and counted throughout the stimulation period. RM one-way ANOVA with Holm-Sidak's
265 post-hoc test was implemented to quantify significance in proliferative events normalized to initial
266 densities for each condition.
267

268 **RESULTS**

269 **$G\alpha_q$-receptor activation induces ER-Ca^{2+} responses and SOCE in hOPC.**

270 We hypothesized that $G\alpha_q$-coupled receptors would exert distinct effects on intracellular calcium
271 responses in hOPCs and that these responses would correlate with their functional effects. Using RNA-
272 seq of human primary PDGFRα-isolated OPCs, we determined that hOPCs expressed a diverse set of
273 122 GPCRs including 14 GPCRs that couple via $G\alpha_q$ proteins (GPCRs "GO:0004930" and PLC activating
274 $G\alpha_q$-coupled "GO:0007200", respectively). To determine the patterns of $G\alpha_q$-mediated calcium responses
275 in hOPCs, we used lentivirus to express the intracellular calcium reporter GCaMP6s hOPCs. We next
276 exposed independent cultures to receptor selective ligands at 10-fold the reported EC_{50} concentration
277 and measured resultant calcium responses (**Fig. 1** and **Table 2**). All ligands induced a detectable
278 increase in intracellular calcium concentration measured by GCaMP6s fluorescence. However,
279 consistent with receptor heterogeneity, the majority of ligands tested increased calcium in only a small
280 fraction of GCaMP6-expressing hOPCs (between 1-30%). In contrast, activation of $M_{1/3}R$ and $mGluR_5$
281 receptors by Oxo-M and CHPG, respectively, elicited robust responses in >46% of hOPCs (n = 3 human
282 samples). Both agonists induced a dose-dependent increase in the proportion of responding cells (**Fig.
283 1C-D**). The extent of total calcium flux was determined by measuring the area-under-curve (AUC). AUC
284 was defined as the area of the response above baseline beginning at the initial response until the end of
285 the imaging session (see methods). Raw AUC values were log_{10}-normalized to achieve normality and
286 displayed as mean ± SEM of pooled responses from >250 cells quantified per each dose from three
287 independent experiments using three independent human samples. Both agonists induced a clear dose-
288 dependent intracellular calcium response with EC_{50} determined as 2.2 μM and 1.3 mM for Oxo-M and
289 CHPG respectively (**Fig. 1E-F**).

290 The calcium responses to $G\alpha_q$-specific agonists were further classified into monotonic and
291 oscillatory responses (**Table 2**). Intriguingly, of those ligands which resulted in calcium transients in <30%
292 of cells, we often observed that the majority of responses were monotonic and typically short-lived
293 returning to baseline within 3 mins following agonist application. In contrast, agonists for $M_{1/3}R$ and
294 $mGluR_5$ receptors resulted in prolonged oscillatory calcium transients which persisted for over nine
295 minutes (9.5 ± 2.0 and 11.0 ± 0.6 mins, for Oxo-M and CHPG respectively; mean ± SEM, n=3 human
296 samples). For all doses tested, Oxo-M elicited oscillatory calcium signals in ~50% of all responsive cells
297 (**Supplementary Fig. S1A**). In comparison, cells responsive to CHPG treatment exhibited a significant
298 increase in the percentage of oscillatory responsive cells at higher concentrations (75μM vs 2300μM, RM
299 one way ANOVA with Holm-Sidak's post-hoc test, $p<0.05$) (**Supplementary Fig. S1B**). The number of
300 oscillations did not differ significantly between Oxo-M nor CHPG concentrations tested (**Supplementary**

301 **Fig. S1C, D**). There was a significant increase in maximum amplitude with Oxo-M dose (main effect,
302 p=0.03), which was not observed in CHPG treated cells (**Supplementary Fig. S1E, F**). Both ligands
303 induced oscillatory calcium signals with an average frequency of ~10 mHz (**Supplementary Fig. S1G,**
304 **H**). As such, the calcium responses following activation of $G\alpha_q$-coupled receptors were distinguishable
305 from one another, and the similarity of prolonged oscillations in the calcium response following $mGluR_5$
306 agonist treatment to $M_{1/3}R$ suggested that a common downstream signaling pathway may be engaged
307 compared to other ligands.

308 As $M_{1/3}R$ activation leads to a profound blockade of hOPC differentiation [12], we hypothesized that
309 the prolonged oscillatory calcium response may underlie this effect and that $mGluR_5$ activation would
310 therefore lead to a similar inhibition of differentiation. In addition, we predicted that EDNRB activation,
311 which instead elicits a minimal and transient calcium response, would not influence hOPC differentiation.
312 To test this hypothesis, we treated hOPCs with ET-1 or CHPG in the absence of mitogens and determined
313 the effect on $O4^+$ oligodendrocyte (OL) differentiation after 3-4 days (**Supplementary Fig. S2**). 150 nM
314 and 1.5 μM ET-1 did not influence the proportion of $O4^+$ OLs (RM One-way ANOVA with Holm-Sidak's
315 post-hoc test, p=0.64, n = 2 human samples) (**Supplemental Fig. S2A, B**). Furthermore, ET-1 did not
316 alter the generation of complex branched $O4^+$ oligodendrocytes (p=0.59) (**Supplemental Fig. S2C**). In
317 contrast, treatment with the $mGluR_5$ agonist CHPG [1.3mM] significantly attenuated $O4^+$ OL
318 differentiation from 42 ± 4% to 32 ± 5% (**Supplemental Fig. S2D, E**)**;** RM One-way ANOVA with Holm-
319 Sidak's post-hoc test, p=0.01, n=5 human samples). Furthermore, CHPG treatment significantly reduced
320 complex branch formation in differentiated $O4^+$ immature oligodendrocytes from 27 ± 4% to 18 ± 5%
321 (p=0.006) suggesting blockade of OL maturation (**Supplemental Fig. S2F**). These data suggest that
322 distinct patterns of calcium signaling occur following $G\alpha_q$-receptor activation and that calcium signaling
323 downstream of $G\alpha_q$-receptor activation may act to block hOPC differentiation and maturation.

324 **SOCE is activated following $M_{1/3}R$ agonist stimulation.**

325 Oscillatory calcium responses can be sustained following endoplasmic reticulum (ER) store
326 release by several mechanisms including calcium recycling and, importantly, by store-operated calcium
327 entry (SOCE) through the activation of calcium release activated channels (CRAC) (for review see[27]).
328 We hypothesized that CRAC channels were activated following $M_{1/3}R$ $G\alpha_q$-receptor activation and store
329 depletion in hOPCs. Calcium responses in hOPCs were measured following infection with lentivirus
330 encoding calcium reporter GCaMP6s [12]. To investigate whether SOCE occurs following ER Ca^{2+}
331 depletion in hOPCs, we treated cells in the absence of extracellular Ca^{2+} with thapsigargin (Tg) [10μM],
332 a sarco-endoplasmic reticulum Ca^{2+}-ATPases inhibitor (SERCA) blocker [43] (**Fig. 1G & Supplemental**
333 **Fig. S3A**). After the initial peak in calcium due to store depletion, we observed a clear SOCE associated

334 peak following the reintroduction of calcium into the media. Pre-incubation with CRAC channel inhibitors
335 2-APB [44] or MRS-1845 [45] substantially reduced SOCE in hOPCs (**Fig. 1G & Supplemental Fig. S3C,**
336 **E**). We quantified SOCE as the area under the calcium curve (AUC) following calcium re-addition (n = 2
337 independent human sample preparations with ≥ 44 cells quantified per condition/replicate). We observed
338 substantial SOCE following ER depletion with Tg (254.5 ± 51.3 AUC arbitrary units) which was nearly
339 abolished by pre-incubation with 2-APB or MRS-1845 (**Fig. 1H;** RM one-way ANOVA with Holm-Sidak's
340 post-hoc test, $p<0.05$; 2-APB: 0.2 ± 0.02; MRS: 7.1± 4.3**).** There were no differences in the initial cytosolic
341 calcium release following Tg induced ER depletion in each condition (RM one-way ANOVA, AUC,
342 $p=0.42$). Together these results were consistent with robust SOCE in hOPCs following ER-depletion that
343 could be blocked by pharmacological CRAC channel antagonists.

344 To test the hypothesis that $M_{1/3}R$ activation leads directly to SOCE, we assessed SOCE following
345 muscarinic agonist treatment. Similar to Tg treatment, Oxo-M [25μM] induced robust SOCE following
346 calcium reintroduction (**Fig. 1G-H & Supplemental Fig. S3B;** 326 ± 67.72 AUC, n = 3 human sample,
347 with ≥48 cells quantified per condition/replicate). Likewise, pre-incubation with 2-APB similarly resulted
348 in a substantial reduction of SOCE (**Fig. 1G-H & Supplemental Fig. S3D;** RM one-way ANOVA with
349 Holm-Sidak's post-hoc test, $p=0.037$; Oxo-M+2-APB: 9.8 ± 3.9). While not significant, we also observed
350 a ~50% reduction in SOCE following pre-incubation with MRS (**Fig. 1G-H & Supplemental Fig. S3F,**
351 Oxo-M+MRS: 169.3 ± 53.8, $p=0.1$). As above, there were no differences in the magnitude of intracellular
352 calcium release following ER-depletion between all Oxo-M conditions tested (RM one-way ANOVA,
353 $p=0.2$). Together, these results show that robust SOCE occurs following $M_{1/3}R$ induced signaling in
354 hOPCs.

355 **STIM1/2 expression is necessary for muscarinic receptor induced SOCE.**

356 The permeability of CRAC channels are regulated by STIM calcium sensor proteins [27]. RNA-seq
357 analyses of human OPCs revealed expression of both calcium sensors STIM1 and STIM2 (STIM1: 8.69
358 ± 0.004 and STIM2: 30.0 ± 0.56; FPKM ± SEM, n=2) and was similar to that observed previously in
359 mouse OPCs [46] (Stim1: 13.9 ± 1.4 and Stim2: 14.9 ± 0.7). We hypothesized that the calcium sensors
360 STIM1 and STIM2 would be directly involved in regulating calcium influx through CRAC channels
361 following $G\alpha_q$-receptor activation in hOPCs. To test this hypothesis, we used siRNA targeting STIM1
362 and/or STIM2 coupled with calcium imaging. We observed a 70-85% decrease in mRNA expression of
363 STIM1 (**Fig. 2A;** one sample t-test $p<0.0001$) and STIM2 (**Fig. 2B;** STIM2 & STIM1/2: $p<0.0001$)
364 following STIM knockdown (KD) in hOPCs. Interestingly, we also observed a small but significant
365 decrease in STIM1 expression ($p<0.05$) following STIM2 siRNA transfection, as well as a reduction in
366 STIM2 expression following STIM1 siRNA ($p<0.01$). To directly assess the role of STIM proteins in

367 muscarinic receptor-induced SOCE, we assessed calcium influx following extracellular calcium removal
368 and re-addition in the context of STIM1/2 KD and Oxo-M treatment. As shown above we identified robust
369 SOCE downstream Oxo-M stimulation which was effectively blocked by CRAC antagonist 2-APB (n=4
370 independent human fetal sample preparations, RM one-way ANOVA with Holm-Sidak's post-hoc test,
371 p=0.003). STIM1 and STIM1/2 KD significantly reduced SOCE by ~40% (STIM1: p=0.047; STIM1/2: p =
372 0.041) while STIM2 had no effect (p=0.19) (**Fig. 2C-E)**. These results suggest that STIM1 contributes to
373 muscarinic-induced SOCE and is a key component of the endogenous hOPC CRAC apparatus. As
374 STIM1/2 silencing may influence endogenous ER-store calcium content, we analyzed the total calcium
375 flux (AUC) and maximum amplitude of ER calcium store depletion in response to Oxo-M following
376 STIM1/2 KD in the absence of extracellular calcium. RM one-way ANOVA revealed no significant
377 differences in either the AUC (**Supplemental Fig. S4A**, Holm-Sidak's post-hoc tests, p=0.1) or maximum
378 amplitude (**Supplemental Fig. S4B**, p>0.4) of ER store release following STIM KD compared to control
379 cells, indicating that STIM silencing did not influence basal ER calcium store content or the extent of ER-
380 calcium depletion following G_q stimulation.

381 We next sought to investigate the effects of STIM1 and STIM2 KD and their roles in regulation of
382 ligand induced Ca^{2+} oscillations in the presence of extracellular calcium. While STIM1 KD induced a
383 greater reduction in Ca^{2+} release following Oxo-M treatment, knockdown of STIM1 or STIM2 significantly
384 attenuated the magnitude of Ca^{2+} release (**Fig. 2F**; linear model with Tukey's HSD posttest, p<0.0001,
385 n=4 human samples). Intriguingly, STIM2 KD also resulted in a significant reduction in the frequency of
386 Ca^{2+} oscillations (**Fig. 2G**; STIM2: p= 0.002; STIM1/2: p=0.0323) while STIM1 KD had no effect (STIM1:
387 p = 0.7236). We also observed that neither STIM1 KD nor STIM2 KD altered the percentage of oscillatory
388 responsive cells (**Supplemental Fig. S5A,** RM one-way ANOVA, p=0.45) or the maximum oscillatory
389 peak amplitude (**Supplemental Fig. S5B,** p=0.1). Interestingly, the oscillatory response duration of Oxo-
390 M induced calcium responses increased following STIM2 KD (p<0.01) and 2-APB treatment (p<0.0001)
391 compared to control cells (**Supplemental Fig. S5C**). In summary, these results suggest that STIM1 is
392 required for $G\alpha_q$-induced SOCE while STIM2 specifically modulates the frequency of Ca^{2+} oscillations
393 following ligand-mediated SOCE.

394 **STIM2 is required for human oligodendrocyte progenitor differentiation.**

395 To determine whether STIM-dependent calcium oscillations may directly contribute to muscarinic
396 $M_{1/3}R$-mediated inhibition of hOPC differentiation, we assessed the independent effects of STIM1 and
397 STIM2 siRNA treatment and their interactions with Oxo-M treatment on hOPC differentiation *in vitro* by
398 three-way ANOVA (**Fig. 3A**). As shown previously[15], Oxo-M treatment significantly blocked differentiation
399 into $O4^+$ immature OLs (F(1,3)=14.31, p=0.032, n=4 human samples). Both siRNA control and STIM1

siRNA transfected hOPCs showed reduced differentiation in response to Oxo-M (**Fig. 3B;** Holm-Sidak's post-hoc test, control: p = 0.006; STIM1: p=0.015). Interestingly, STIM2 siRNA transfection alone or in combination with STIM1 abolished the anti-differentiative effects of Oxo-M (p > 0.2). This is consistent with a role of STIM2 downstream of Oxo-M mediated signaling.

In addition to Oxo-M dependent effects, STIM2 siRNA alone caused a significant reduction in $O4^+$ OL differentiation (RM three-way ANOVA, STIM2 main effect F(1,3) = 28.64, p = 0.013, n=4 human samples) while STIM1 siRNA had no effect (p = 0.42). In the absence of Oxo-M, we observed a significant decrease in $O4^+$ OL differentiation cells following STIM2 siRNA transfection relative to siControl (p=0.002). Interestingly, this effect was not observed when STIM1/2 siRNA were combined (p>0.05). These results suggested that STIM2 signaling in the absence of $G\alpha_q$ agonist regulates hOPC differentiation and is required for the anti-differentiative effects of muscarinic agonism. We further examined the effect of STIM1/2 on morphological maturation by assessing the proportion of $O4^+$ cells with simple or complex process elaboration as described [47] (**Supplemental Fig. S6A**). STIM1/2 KD did not influence the percentage of simple $O4^+$ oligodendrocytes (3-way ANOVA, p > 0.3). Oxo-M reduced the proportion of complex $O4^+$ cells following transfection with either control or STIM1 siRNA but did not influence complex $O4^+$ cell number following STIM2 KD (Holm-Sidak's post-hoc test, p < 0.05) (**Supplemental Fig. S6C**). Interestingly, in the absence of Oxo-M, STIM2 KD reduced the percentage of complex $O4^+$ cells (Holm-Sidak's post-hoc test, p =0.0013), while STIM1 KD had no effect (p=0.61).

As differentiation and OPC proliferation are intimately linked, we next examined whether ER calcium sensors STIM1/2 influenced hOPC proliferation. We quantified the proportion of dividing $Ki67^+$ OPCs following transfection with STIM1/2 siRNA or control siRNA (**Fig. 3C**). Similar to previous observations [15], Oxo-M had no effect on hOPC proliferation. STIM1 or STIM2 siRNA treatment did not significantly influence proliferation (n = 3 human samples; three-way ANOVA, STIM1 F(1, 2) = 12.57, p = 0.071, STIM2 F (1, 2) = 6.27, p = 0.12). Taken together, these data suggest that STIM2 appears to be necessary for OL differentiation and morphological maturation and may be required for the effects of muscarinic agonist-mediated inhibition.

Optogenetically-induced SOCE blocks hOPC differentiation and promotes proliferation.

Our previous results suggest that STIM1/2 mediated SOCE may be required for sustained calcium release following $G\alpha_q$ stimulation and thereby contribute to muscarinic inhibition of differentiation. We therefore sought to test whether oscillatory calcium SOCE directly regulates hOPC development. To this end, we expressed an optogenetically controllable STIM protein in hOPCs to enable blue-light control of SOCE in the absence of $G\alpha_q$-ligand stimulation [37]. Following infection with lentiviral OptoSTIM, hOPCs were transduced with lentiviral jRCaMP1a, a red-shifted calcium indicator, to simultaneously measure

433 intracellular Ca^{2+} while induced SOCE [35]. Blue light activation of OptoSTIM resulted in a consistent and
434 robust oscillatory calcium influx which could be sustained for several hours in a frequency-specific
435 manner (**Fig. 4A-B**). To avoid summation of OptoSTIM-induced Ca^{2+} release and ensure a distinct
436 oscillatory wave form, based on the dissociation kinetics of OptoSTIM [37], we selected an upper frequency
437 of 3.33 mHz to model that of 10mHz waves observed following muscarinic receptor activation. As a
438 control, we selected a lower frequency of 0.55 mHz which is below the lower threshold associated with
439 frequency-dependent decoding in other non-excitable cells [28,48]. We matched the total blue-light exposure
440 over time between frequencies by pulsing for 330 and 2000 ms seconds at 3.33 and 0.55 mHz
441 respectively. Based on jRCaMP1a imaging, oscillatory SOCE could be maintained for at least three hours
442 in hOPCs *in vitro* and was clearly observable at 18 hours with 2000 ms pulses without loss of signal (**Fig.**
443 **4B**, n = 3 human samples). Importantly, we found that the total calcium release defined by AUC over the
444 2.5 h period was equivalent between groups (**Fig. 4C**; RM one-way ANOVA, Holm-Sidak's post-hoc test,
445 p = 0.49). As such, we could assess frequency dependent SOCE effects while controlling for total calcium
446 flux.

447 We examined the effect of optogenetically-induced oscillatory SOCE on hOPC proliferation and
448 differentiation (**Fig. 5**). Using time lapse microscopy and concurrent intermittent blue-light stimulation to
449 induce SOCE, we assessed the number of mitotic events (**Fig. 5A**) that occurred in the presence of both
450 high and low frequency OptoSTIM1-induced SOCE. Induction of high frequency (3.33 mHz) oscillatory
451 calcium entry produced a clear increase in the number of cumulative mitotic events at 24h and 36h post
452 stimulation respectively (**Fig. 5B**, quantified in **C**; RM one-way ANOVA with Holm-Sidak's post-hoc test,
453 p = 0.006, n = 4 human samples). After 36 hours of stimulation, high frequency SOCE resulted in a 40%
454 increase rate of cell division relative to unstimulated control hOPCs (3.33 mHz: 25.6 ± 4.9% vs. control:
455 19.1 ± 4.7%, p = 0.014) (**Fig. 5C**). In contrast, low frequency SOCE had no effect on proliferation (0.55
456 mHz; 17.6 ± 5.9%, p = 0.38). Next, we investigated the effects of long term OptoSTIM induction on hOPC
457 differentiation (**Fig. 5D**). We observed no gross alterations in transduced cell number following blue-light
458 stimulation (**Fig. 5E**; RM one-way ANOVA with Holm-Sidak's post-hoc test, p = 0.90, n = 4 human
459 samples). Importantly, induction of high frequency SOCE substantially impaired hOPC differentiation by
460 50% relative to unstimulated control hOPCs (**Fig. 5F**; 3.33 mHz: 7.5 ± 1.7% $O4^+/GFP^+$ cells vs. control:
461 16.6 ± 3.4, p = 0.02). Differentiation by hOPCs which received induction of low frequency SOCE was not
462 significantly different from unstimulated control cells (0.55 mHz: 12.83 ± 3.3%). Moreover, there was a
463 significant reduction in the number of $O4^+$ cells with complex branch morphology (>3 processes) following
464 3.33 mHz stimulation compared to control cells (**Fig. 5G;** RM one-way ANOVA with Holm-Sidak's post-
465 hoc test, p = 0.04). This suggests that induction of oscillatory SOCE was sufficient to inhibit hOPC

466 morphological maturation. Collectively these results indicate that sustained high frequency oscillatory
467 SOCE was sufficient to both block hOPC differentiation and augment hOPC proliferation.

468 **DISCUSSION**

469 In the present study, we demonstrate that a subset of $G\alpha_q$-receptors expressed by human primary
470 OPCs, including muscarinic M_1 and M_3 receptors ($M_{1/3}R$) and metabotropic-glutamate-receptor-5
471 (mGluR5), induced prolonged oscillatory calcium signaling and that the ability to induce oscillatory
472 calcium signaling correlated with their capacity to block differentiation. We found that a shared
473 mechanism downstream muscarinic $G\alpha_q$-receptor induced oscillatory signaling was the activation of store
474 operated calcium entry (SOCE). Inhibition with SOCE antagonists or knockdown of ER-localized SOCE
475 calcium sensors STIM1/2 reduced the magnitude of calcium signaling induced by muscarinic agonist
476 stimulation. STIM2 ablation selectively reduced calcium oscillation frequency and spontaneous OL
477 differentiation *in vitro* and, unlike control OPCs, treatment with muscarinic ligand did not further reduce
478 differentiation following STIM2 knockdown. While SOCE exerted a major influence on calcium
479 oscillations, as these experiments were performed using constant $G\alpha_q$-receptor agonist exposure, we
480 cannot exclude the requirement of IP_3-mediated release for the maintenance of prolonged calcium
481 oscillations. Together, these data suggested a functional linkage between muscarinic receptor signaling
482 and SOCE. Using an optogenetic approach to selectively activate SOCE in OPCs, we found that SOCE
483 was sufficient to modulate OL differentiation in the absence of $G\alpha_q$ dependent signaling suggesting that
484 SOCE is a key facet that impairs OL differentiation and remyelination. Furthermore, the frequency of
485 SOCE rather than the overall amount of calcium influx due to SOCE was found to be vital in mediating
486 the effect of calcium entry on differentiation and proliferation. This suggests that the calcium pathway
487 includes frequency-dependent 'decoders' which regulate OL differentiation and that modulation of
488 calcium frequency might represent an important mechanism by which diverse signals are integrated by
489 parenchymal OPCs.

490 In drug development, G-protein coupled receptors (GPCRs) are attractive candidates for
491 therapeutic intervention and recently many small molecules that target GPCRs have been identified that
492 modulate OPC function and OL differentiation to promote myelin repair [49]. For example, GPR17 which
493 largely couples via $G\alpha_{i/o}$ was found to negatively regulate OPC differentiation while knockout was
494 observed to promote remyelination [50]. Muscarinic receptor antagonists have displayed a remarkable
495 capacity to improve OL differentiation and remyelination in various animal models. Using genetic
496 approaches, the effects of these drugs have been localized to M_1R and M_3R. Both of these receptors
497 represent canonical $G\alpha_q$-coupled receptors. Indeed, when Gα coupling was systematically analyzed
498 across different subunits, M_3R displayed exquisite selectivity for rapid activation for $G\alpha_q/G\alpha_{11}$ coupling [51].
499 In this study, we focused on $G\alpha_q$-coupled receptors to determine if a shared characteristic of $G\alpha_q$
500 receptors could be used to predict their ability to prevent efficient OL differentiation and thereby impair
501 remyelination. We analyzed RNA-seq analysis of primary hOPC to identity those $G\alpha_q$-coupled receptors

502 expressed at the mRNA level and hypothesized that receptor-specific ligand activation would produce
503 canonical oscillatory calcium signaling and block hOPC differentiation. Surprisingly, only a small subset
504 of pharmacological $G\alpha_q$ ligands were capable of inducing prolonged calcium oscillation in hOPCs.
505 Intriguingly, this correlated with the ability of ligands to effectively block OL differentiation. CHPG, which
506 activates $mGluR_5$ in a highly selective manner, was the only other ligand capable of inducing calcium
507 oscillations in a large fraction of hOPCs. The specificity of $G\alpha_q$-receptor mediated signaling is consistent
508 with previous results which have shown that while endothelin (ET) agonist treatment induces a monotonic
509 calcium response [24] while metabotropic glutamate receptor agonists induce calcium oscillations [19].
510 $mGluR_5$ couples primarily via $G\alpha_q$ and does not have appreciable activity at $G\alpha_i$. In a similar manner to
511 M_3R, $mGluR_5$ mRNA was relatively highly expressed in rodent OPCs and down-regulated following
512 differentiation [19]. Herein, we found that treatment with CHPG resulted in a dose-dependent blockade of
513 hOPC differentiation.

514 In contrast, the other $G\alpha_q$ couple receptors that elicited calcium responses in OPCs induced
515 calcium release that was either considerably shorter in duration and/or were largely monotonic in nature.
516 These differences could be due to differences in overall level of expression and/or differences in receptor
517 coupling. From a large-scale screen of G-protein coupling [52], we observed that many of these receptors
518 were promiscuously coupled with other Gα subunits. For example, sphingosine-1-phosphate-receptor-1
519 (S1PR1) was observed as primarily coupled via $G\alpha_i$ and $G\alpha_o$ with little evidence of $G\alpha_q$ coupling. This
520 difference corresponded with the observed function difference following activation of S1PR1 which results
521 in OL differentiation from human OPCs [53]. Furthermore, endothelin-B receptor (ENDRB), thrombin
522 receptor II (F2R) and purinergic receptor Y1 (P2RY1) also show promiscuous coupling with multiple Gα
523 proteins upon activation. Together this suggests that selectively in coupling may influence the net
524 influence on downstream signaling and the nature of the resultant calcium response. As the coupling of
525 GPCRs to specific Gα proteins are not absolute and in many cases is promiscuous, we anticipate that
526 biased ligands or antagonists capable of promoting or blocking coupling along specific pathways may
527 represent optimal approaches to promote OPC differentiation.

528 The mechanisms which shape the calcium-response following ligand application are complex and
529 likely dependent on multiple interacting proteins. Among these, Gα subunits form specific complexes with
530 their cognate Gβγ proteins which possess their own signaling capability and modulate the signaling of Gα
531 subunits they interact with [54]. Among these, specific isoforms of phosphoinositide 3-kinase (PI3K) and
532 adenylate cyclase, voltage-operated calcium channels (VOCC) and inwardly rectifying K^+ channel can
533 be regulated by Gβγ. Activation of PI3K/Akt [55], adenylate cyclase [56], and VOCC [57] are associated with
534 promotion of OPC differentiation suggesting that Gβγ activation may counteract oscillatory calcium
535 signaling. For muscarinic receptor signaling, in rat pituitary cells $G_{\beta 3}$ is necessary for the carbachol-

536 mediated calcium current [58], while in a rat leukemia cell line $G_{\beta1}$ and $G_{\beta4}$ were more important in the
537 regulation of this current [59]. In primary hOPCs, $G_{\beta4}$ ablation did not influence calcium signaling following
538 Oxo-M treatment [60], though redundancy with $G_{\beta1}$ and $G_{\beta2}$ is possible as these subunits are expressed at
539 substantially higher levels in human, rat, and mouse OPCs.

540 In addition to the $G_{\beta\gamma}$ subunit specific regulation, receptor-specific activation of regulators of G-
541 protein signaling (RGS) proteins provide specificity for G-protein coupling and modulate the kinetics of
542 second messenger activation [61]. RGS proteins promote termination of GPCR signaling via GTPase
543 activation and prevent GPCR signaling in the absence of ligand. Following ligand activation and elevated
544 Ca^{2+}, RGS proteins exhibit a cyclical pattern of association with phosphatidylinositol-3,4,5-trisphosphate
545 (PIP_3) and activated calcium/calmodulin (Ca^{2+}/CaM) followed by re-association with the GPCR complex
546 after Ca^{2+} levels return to baseline. This allows a second cycle to start and initiate another calcium spike.
547 The kinetics of these steps, especially the slow dissociation of RGS protein from Ca^{2+}/CaM, contributes
548 to the resultant frequency of calcium oscillations [62]. While the role of specific RGS proteins in the OPC
549 and OL lineage is poorly understood, several RGS proteins are expressed in OPCs [46]. Among these,
550 RGS4 has been shown to be a potent negative regulator of muscarinic receptor signaling in insulinoma
551 cells [63]. Also noteworthy, the R7 family of RGS proteins (RGS6/7/9/11) form heterodimers with G-protein
552 β subunit Gβ5 (GNB5) which similarly attenuates M_3R-dependent Ca^{2+} signaling [64].

553 Once activated, SOCE is associated with many cellular functions in neural progenitors such as
554 proliferation [65] and differentiation [66,67]. In OPCs, SOCE can modulate PDGF-AA induced OPC
555 proliferation [30]. However, given the known role of PI3K/Akt signaling downstream of PDGF receptor,
556 SOCE is unlikely to be a critical component of PDGF signaling. Likewise, the cellular role of calcium
557 oscillations in OPC soma is not yet known. Our data using optogenetic induction of SOCE strongly
558 suggest that oscillatory SOCE alone is sufficient to modulate both OPC proliferation and differentiation.
559 While we were limited by the dissociation kinetics of OptoSTIM to an upper limit of 3.33 mHz stimulation,
560 this frequency fits within the known frequencies of calcium oscillations in non-excitable cells and may
561 recruit NFAT, NFκB and other downstream pathways [48]. By matching total calcium influx during the period
562 of exposure, we were able to demonstrate frequency dependence as a substantially lower frequency
563 (0.55 mHz) was unable to modulate proliferation or differentiation. New approaches will be required to
564 determine whether higher frequency SOCE can further alter these critical cellular processes.

565 SOCE itself is dependent on the association of CRAC subunit comprising STIM ER-calcium
566 sensors and ORAI channel subunits. While STIM1 and STIM2 contributed to different aspects of
567 muscarinic-induced SOCE and sustained oscillatory calcium signaling in hOPCs, we found that only
568 STIM2 knockdown reduced spontaneous OL differentiation. Previous reports have found that apart from
569 its role in agonist mediated SOCE, STIM2 signaling often persists to a lesser degree in the absence of

570 an ER-release stimulus. STIM2 responds to small fluctuations in ER calcium levels, and drives small local
571 SOCE calcium entry when local calcium levels fall below baseline (reviewed in [68]). It is also known that
572 STIM2 can regulate endogenous differentiation of other cell types through modulation of cytoplasmic
573 calcium levels following STIM1-induced oscillatory SOCE [69]. Furthermore, small spontaneous SOCE
574 calcium transients in the absence of agonist have been observed in mouse OPCs, and have been
575 implicated in the regulation of differentiation [70]. It is possible, therefore, that STIM2 is required for these
576 spontaneous transients and thus STIM2 KD may inhibit differentiation. In contrast, our data is consistent
577 with prolonged oscillatory SOCE, either produced optogenetically or in response to M_3R and $mGluR_5$
578 agonists, causing a blockade of hOPC differentiation via global calcium-mediated changes. Additional
579 studies will be necessary to tease apart the specific mechanisms by which STIM2 directly influences
580 oligodendrocyte differentiation.

581 The ER-calcium sensors STIM1/2 physically and functionally interact with one another to regulate
582 SOCE [68]. The relative abundance of STIM1 and STIM2 vary greatly between tissues and individual cell
583 types. In human OPCs, STIM2 is more than 3-fold more abundant than STIM1 mRNA but both genes are
584 relatively highly expressed (>10 FPKM). In contrast, both STIM1 and STIM2 are expressed at equivalent
585 levels in mouse OPCs [46]. As the differences in the relative expression of STIM1/2 influences the resultant
586 properties of SOCE in response to store depletion (reviewed in [71]), the differences in STIM1:STIM2 ratio
587 in mouse and human may therefore underlie some of the species-specific functional differences in OPC
588 behavior [72]. Both STIM1 and STIM2 have been shown to contribute to oscillatory SOCE in a context
589 dependent manner [73,74]. Our data support a specific role of STIM2 in the regulation of OPC calcium
590 oscillations and suggest that expression of STIM2 is required for muscarinic receptor induced
591 differentiation blockade in hOPCs. Together with the direct regulation of OPC differentiation via
592 optogenetically-gated SOCE, these data suggest that SOCE mediated via STIM activation will likely play
593 an important role in mediating the negative effects of $G\alpha_q$-coupled receptors capable of blocking
594 oligodendrocyte differentiation in health and disease.
595
596

597 **REFERENCES**

598 1 Franklin, R. J. M. & Ffrench-Constant, C. Regenerating CNS myelin - from mechanisms to
599 experimental medicines. *Nature reviews. Neuroscience* **18**, 753-769, doi:10.1038/nrn.2017.136
600 (2017).
601 2 Faissner, S., Plemel, J. R., Gold, R. & Yong, V. W. Progressive multiple sclerosis: from
602 pathophysiology to therapeutic strategies. *Nat Rev Drug Discov* **18**, 905-922,
603 doi:10.1038/s41573-019-0035-2 (2019).
604 3 Kuhlmann, T. *et al.* Differentiation block of oligodendroglial progenitor cells as a cause for
605 remyelination failure in chronic multiple sclerosis. *Brain : a journal of neurology* **131**, 1749-1758,
606 doi:10.1093/brain/awn096 (2008).
607 4 Wolswijk, G. Chronic stage multiple sclerosis lesions contain a relatively quiescent population of
608 oligodendrocyte precursor cells. *J Neurosci* **18**, 601-609 (1998).
609 5 Thornton, M. A. & Hughes, E. G. Neuron-oligodendroglia interactions: Activity-dependent
610 regulation of cellular signaling. *Neuroscience letters* **727**, 134916,
611 doi:10.1016/j.neulet.2020.134916 (2020).
612 6 Ortiz, F. C. *et al.* Neuronal activity in vivo enhances functional myelin repair. *JCI Insight* **5**,
613 doi:10.1172/jci.insight.123434 (2019).
614 7 Gautier, H. O. *et al.* Neuronal activity regulates remyelination via glutamate signalling to
615 oligodendrocyte progenitors. *Nat Commun* **6**, 8518, doi:10.1038/ncomms9518 (2015).
616 8 Bernstein, M., Lyons, S. A., Moller, T. & Kettenmann, H. Receptor-mediated calcium signalling
617 in glial cells from mouse corpus callosum slices. *Journal of neuroscience research* **46**, 152-163,
618 doi:10.1002/(SICI)1097-4547(19961015)46:2<152::AID-JNR3>3.0.CO;2-G (1996).
619 9 Paez, P. M. & Lyons, D. A. Calcium Signaling in the Oligodendrocyte Lineage: Regulators and
620 Consequences. *Annual review of neuroscience* **43**, 163-186, doi:10.1146/annurev-neuro-
621 100719-093305 (2020).
622 10 Berridge, M. J. & Irvine, R. F. Inositol phosphates and cell signalling. *Nature* **341**, 197-205,
623 doi:10.1038/341197a0 (1989).
624 11 Mei, F. *et al.* Accelerated remyelination during inflammatory demyelination prevents axonal loss
625 and improves functional recovery. *Elife* **5**, e18246, doi:10.7554/eLife.18246 (2016).
626 12 Welliver, R. R. *et al.* Muscarinic Receptor M3R Signaling Prevents Efficient Remyelination by
627 Human and Mouse Oligodendrocyte Progenitor Cells. *J Neurosci* **38**, 6921-6932,
628 doi:10.1523/JNEUROSCI.1862-17.2018 (2018).
629 13 Mei, F. *et al.* Micropillar arrays as a high-throughput screening platform for therapeutics in
630 multiple sclerosis. *Nature medicine* **20**, 954-960, doi:10.1038/nm.3618 (2014).

631 14 Deshmukh, V. A. *et al.* A regenerative approach to the treatment of multiple sclerosis. *Nature*
632 **502**, 327-332, doi:10.1038/nature12647 (2013).
633 15 Abiraman, K. *et al.* Anti-muscarinic adjunct therapy accelerates functional human
634 oligodendrocyte repair. *J Neurosci* **35**, 3676-3688, doi:10.1523/JNEUROSCI.3510-14.2015
635 (2015).
636 16 Gadea, A., Aguirre, A., Haydar, T. F. & Gallo, V. Endothelin-1 regulates oligodendrocyte
637 development. *J Neurosci* **29**, 10047-10062, doi:10.1523/JNEUROSCI.0822-09.2009 (2009).
638 17 Agresti, C. *et al.* ATP regulates oligodendrocyte progenitor migration, proliferation, and
639 differentiation: involvement of metabotropic P2 receptors. *Brain Res Brain Res Rev* **48**, 157-
640 165, doi:10.1016/j.brainresrev.2004.12.005 (2005).
641 18 Takeda, M., Nelson, D. J. & Soliven, B. Calcium signaling in cultured rat oligodendrocytes. *Glia*
642 **14**, 225-236, doi:10.1002/glia.440140308 (1995).
643 19 Luyt, K., Varadi, A., Durant, C. F. & Molnar, E. Oligodendroglial metabotropic glutamate
644 receptors are developmentally regulated and involved in the prevention of apoptosis. *J*
645 *Neurochem* **99**, 641-656, doi:10.1111/j.1471-4159.2006.04103.x (2006).
646 20 Fan, L. W. *et al.* Exposure to serotonin adversely affects oligodendrocyte development and
647 myelination in vitro. *J Neurochem* **133**, 532-543, doi:10.1111/jnc.12988 (2015).
648 21 Jung, C. G. *et al.* Functional consequences of S1P receptor modulation in rat oligodendroglial
649 lineage cells. *Glia* **55**, 1656-1667, doi:10.1002/glia.20576 (2007).
650 22 Chattopadhyay, N. *et al.* Calcium receptor expression and function in oligodendrocyte
651 commitment and lineage progression: potential impact on reduced myelin basic protein in CaR-
652 null mice. *Journal of neuroscience research* **86**, 2159-2167, doi:10.1002/jnr.21662 (2008).
653 23 Coppi, E. *et al.* Adenosine A2B receptors inhibit K(+) currents and cell differentiation in cultured
654 oligodendrocyte precursor cells and modulate sphingosine-1-phosphate signaling pathway.
655 *Biochem Pharmacol* **177**, 113956, doi:10.1016/j.bcp.2020.113956 (2020).
656 24 Jung, K. J. *et al.* The role of endothelin receptor A during myelination of developing
657 oligodendrocytes. *J Korean Med Sci* **26**, 92-99, doi:10.3346/jkms.2011.26.1.92 (2011).
658 25 Yuen, T. J. *et al.* Identification of endothelin 2 as an inflammatory factor that promotes central
659 nervous system remyelination. *Brain : a journal of neurology* **136**, 1035-1047,
660 doi:10.1093/brain/awt024 (2013).
661 26 Dukala, D. E. & Soliven, B. S1P1 deletion in oligodendroglial lineage cells: Effect on
662 differentiation and myelination. *Glia* **64**, 570-582, doi:10.1002/glia.22949 (2016).
663 27 Prakriya, M. & Lewis, R. S. Store-Operated Calcium Channels. *Physiol Rev* **95**, 1383-1436,
664 doi:10.1152/physrev.00020.2014 (2015).

665 28 Smedler, E. & Uhlen, P. Frequency decoding of calcium oscillations. *Biochim Biophys Acta*
666 **1840**, 964-969, doi:10.1016/j.bbagen.2013.11.015 (2014).
667 29 Samanta, K. & Parekh, A. B. Spatial Ca(2+) profiling: decrypting the universal cytosolic Ca(2+)
668 oscillation. *J Physiol* **595**, 3053-3062, doi:10.1113/JP272860 (2017).
669 30 Paez, P. M. *et al.* Regulation of store-operated and voltage-operated Ca2+ channels in the
670 proliferation and death of oligodendrocyte precursor cells by golli proteins. *ASN Neuro* **1**,
671 doi:10.1042/AN20090003 (2009).
672 31 Schmidt, C., Ohlemeyer, C., Kettenmann, H., Reutter, W. & Horstkorte, R. Incorporation of N-
673 propanoylneuraminic acid leads to calcium oscillations in oligodendrocytes upon the application
674 of GABA. *Febs Letters* **478**, 276-280, doi:Doi 10.1016/S0014-5793(00)01868-8 (2000).
675 32 Paez, P. M., Fulton, D., Spreuer, V., Handley, V. & Campagnoni, A. T. Modulation of canonical
676 transient receptor potential channel 1 in the proliferation of oligodendrocyte precursor cells by
677 the golli products of the myelin basic protein gene. *J Neurosci* **31**, 3625-3637,
678 doi:10.1523/JNEUROSCI.4424-10.2011 (2011).
679 33 Conway, G. D., O'Bara, M. A., Vedia, B. H., Pol, S. U. & Sim, F. J. Histone deacetylase activity
680 is required for human oligodendrocyte progenitor differentiation. *Glia* **60**, 1944-1953,
681 doi:10.1002/glia.22410 (2012).
682 34 Pol, S. U. *et al.* Sox10-MCS5 enhancer dynamically tracks human oligodendrocyte progenitor
683 fate. *Experimental neurology* **247**, 694-702, doi:10.1016/j.expneurol.2013.03.010 (2013).
684 35 Dana, H. *et al.* Sensitive red protein calcium indicators for imaging neural activity. *Elife* **5**,
685 doi:10.7554/eLife.12727 (2016).
686 36 Sevin, C. *et al.* Intracerebral adeno-associated virus-mediated gene transfer in rapidly
687 progressive forms of metachromatic leukodystrophy. *Hum Mol Genet* **15**, 53-64,
688 doi:10.1093/hmg/ddi425 (2006).
689 37 Kyung, T. *et al.* Optogenetic control of endogenous Ca(2+) channels in vivo. *Nature*
690 *biotechnology* **33**, 1092-1096, doi:10.1038/nbt.3350 (2015).
691 38 Wang, J. *et al.* Paired Related Homeobox Protein 1 Regulates Quiescence in Human
692 Oligodendrocyte Progenitors. *Cell reports* **25**, 3435-3450 e3436,
693 doi:10.1016/j.celrep.2018.11.068 (2018).
694 39 Geraerts, M., Willems, S., Baekelandt, V., Debyser, Z. & Gijsbers, R. Comparison of lentiviral
695 vector titration methods. *BMC biotechnology* **6**, 34, doi:10.1186/1472-6750-6-34 (2006).
696 40 Edelstein, A., Amodaj, N., Hoover, K., Vale, R. & Stuurman, N. Computer control of
697 microscopes using microManager. *Current protocols in molecular biology* **Chapter 14**,
698 Unit14.20, doi:10.1002/0471142727.mb1420s92 (2010).

699 41 Stockley, J. H. *et al.* Surpassing light-induced cell damage in vitro with novel cell culture media.
700 *Sci Rep* **7**, 849, doi:10.1038/s41598-017-00829-x (2017).
701 42 Tinevez, J. Y. *et al.* TrackMate: An open and extensible platform for single-particle tracking.
702 *Methods* **115**, 80-90, doi:10.1016/j.ymeth.2016.09.016 (2017).
703 43 Treiman, M., Caspersen, C. & Christensen, S. B. A tool coming of age: thapsigargin as an
704 inhibitor of sarco-endoplasmic reticulum Ca(2+)-ATPases. *Trends in pharmacological sciences*
705 **19**, 131-135, doi:10.1016/s0165-6147(98)01184-5 (1998).
706 44 DeHaven, W. I., Smyth, J. T., Boyles, R. R., Bird, G. S. & Putney, J. W., Jr. Complex actions of
707 2-aminoethyldiphenyl borate on store-operated calcium entry. *The Journal of biological*
708 *chemistry* **283**, 19265-19273, doi:10.1074/jbc.M801535200 (2008).
709 45 Harper, J. L. *et al.* Dihydropyridines as inhibitors of capacitative calcium entry in leukemic HL-60
710 cells. *Biochem Pharmacol* **65**, 329-338, doi:10.1016/s0006-2952(02)01488-0 (2003).
711 46 Zhang, Y. *et al.* An RNA-sequencing transcriptome and splicing database of glia, neurons, and
712 vascular cells of the cerebral cortex. *J Neurosci* **34**, 11929-11947,
713 doi:10.1523/JNEUROSCI.1860-14.2014 (2014).
714 47 Huang, J. K. *et al.* Retinoid X receptor gamma signaling accelerates CNS remyelination. *Nat*
715 *Neurosci* **14**, 45-53, doi:10.1038/nn.2702 (2011).
716 48 Boulware, M. J. & Marchant, J. S. Timing in cellular Ca2+ signaling. *Curr Biol* **18**, R769-R776,
717 doi:10.1016/j.cub.2008.07.018 (2008).
718 49 Mogha, A., D'Rozario, M. & Monk, K. R. G Protein-Coupled Receptors in Myelinating Glia.
719 *Trends in pharmacological sciences* **37**, 977-987, doi:10.1016/j.tips.2016.09.002 (2016).
720 50 Ou, Z. *et al.* Olig2-Targeted G-Protein-Coupled Receptor Gpr17 Regulates Oligodendrocyte
721 Survival in Response to Lysolecithin-Induced Demyelination. *J Neurosci* **36**, 10560-10573,
722 doi:10.1523/JNEUROSCI.0898-16.2016 (2016).
723 51 Masuho, I. *et al.* Distinct profiles of functional discrimination among G proteins determine the
724 actions of G protein-coupled receptors. *Sci Signal* **8**, ra123, doi:10.1126/scisignal.aab4068
725 (2015).
726 52 Inoue, A. *et al.* Illuminating G-Protein-Coupling Selectivity of GPCRs. *Cell* **177**, 1933-1947
727 e1925, doi:10.1016/j.cell.2019.04.044 (2019).
728 53 Cui, Q. L., Fang, J., Kennedy, T. E., Almazan, G. & Antel, J. P. Role of p38MAPK in S1P
729 receptor-mediated differentiation of human oligodendrocyte progenitors. *Glia* **62**, 1361-1375,
730 doi:https://doi.org/10.1002/glia.22688 (2014).

731 54 Khan, S. M. *et al.* The expanding roles of Gbetagamma subunits in G protein-coupled receptor
732 signaling and drug action. *Pharmacological reviews* **65**, 545-577, doi:10.1124/pr.111.005603
733 (2013).
734 55 Goebbels, S. *et al.* Elevated phosphatidylinositol 3,4,5-trisphosphate in glia triggers cell-
735 autonomous membrane wrapping and myelination. *J Neurosci* **30**, 8953-8964,
736 doi:10.1523/jneurosci.0219-10.2010 (2010).
737 56 Raible, D. W. & McMorris, F. A. Induction of oligodendrocyte differentiation by activators of
738 adenylate cyclase. *Journal of neuroscience research* **27**, 43-46,
739 doi:https://doi.org/10.1002/jnr.490270107 (1990).
740 57 Cheli, V. T. *et al.* Conditional Deletion of the L-Type Calcium Channel Cav1.2 in
741 Oligodendrocyte Progenitor Cells Affects Postnatal Myelination in Mice. *J Neurosci* **36**, 10853-
742 10869, doi:10.1523/JNEUROSCI.1770-16.2016 (2016).
743 58 Kleuss, C., Scherübl, H., Hescheler, J., Schultz, G. & Wittig, B. Different β-subunits determine
744 G-protein interaction with transmembrane receptors. *Nature* **358**, 424-426,
745 doi:10.1038/358424a0 (1992).
746 59 Dippel, E., Kalkbrenner, F., Wittig, B. & Schultz, G. A heterotrimeric G protein complex couples
747 the muscarinic m1 receptor to phospholipase C-beta. *Proceedings of the National Academy of*
748 *Sciences* **93**, 1391-1396, doi:10.1073/pnas.93.4.1391 (1996).
749 60 Pol, S. U. *et al.* Network-Based Genomic Analysis of Human Oligodendrocyte Progenitor
750 Differentiation. *Stem cell reports* **9**, 710-723, doi:10.1016/j.stemcr.2017.07.007 (2017).
751 61 Kach, J., Sethakorn, N. & Dulin, N. O. A finer tuning of G-protein signaling through regulated
752 control of RGS proteins. *Am J Physiol Heart Circ Physiol* **303**, H19-35,
753 doi:10.1152/ajpheart.00764.2011 (2012).
754 62 Luo, X., Popov, S., Bera, A. K., Wilkie, T. M. & Muallem, S. RGS Proteins Provide Biochemical
755 Control of Agonist-Evoked [Ca2+]i Oscillations. *Molecular cell* **7**, 651-660,
756 doi:https://doi.org/10.1016/S1097-2765(01)00211-8 (2001).
757 63 Ruiz de Azua, I. *et al.* RGS4 is a negative regulator of insulin release from pancreatic β-cells in
758 vitro and in vivo. *Proceedings of the National Academy of Sciences* **107**, 7999-8004,
759 doi:10.1073/pnas.1003655107 (2010).
760 64 Karpinsky-Semper, D., Volmar, C. H., Brothers, S. P. & Slepak, V. Z. Differential effects of the
761 Gβ5-RGS7 complex on muscarinic M3 receptor-induced Ca2+ influx and release. *Mol*
762 *Pharmacol* **85**, 758-768, doi:10.1124/mol.114.091843 (2014).
763 65 Domenichini, F. *et al.* Store-Operated Calcium Entries Control Neural Stem Cell Self-Renewal in
764 the Adult Brain Subventricular Zone. *Stem Cells* **36**, 761-774, doi:10.1002/stem.2786 (2018).

765 66 Forostyak, O. *et al.* Physiology of Ca(2+) signalling in stem cells of different origins and
766 differentiation stages. *Cell Calcium* **59**, 57-66, doi:10.1016/j.ceca.2016.02.001 (2016).
767 67 Gopurappilly, R., Deb, B. K., Chakraborty, P. & Hasan, G. Stable STIM1 Knockdown in Self-
768 Renewing Human Neural Precursors Promotes Premature Neural Differentiation. *Front Mol*
769 *Neurosci* **11**, 178, doi:10.3389/fnmol.2018.00178 (2018).
770 68 López, E., Salido, G. M., Rosado, J. A. & Berna-Erro, A. Unraveling STIM2 function. *J Physiol*
771 *Biochem* **68**, 619-633, doi:10.1007/s13105-012-0163-1 (2012).
772 69 Darbellay, B. *et al.* Human muscle economy myoblast differentiation and excitation-contraction
773 coupling use the same molecular partners, STIM1 and STIM2. *J Biol Chem* **285**, 22437-22447,
774 doi:10.1074/jbc.M110.118984 (2010).
775 70 Rui, Y., Pollitt, S. L., Myers, K. R., Feng, Y. & Zheng, J. Q. Spontaneous Local Calcium
776 Transients Regulate Oligodendrocyte Development in Culture through Store-Operated Ca(2+)
777 Entry and Release. *eNeuro* **7**, doi:10.1523/ENEURO.0347-19.2020 (2020).
778 71 Berna-Erro, A., Jardin, I., Salido, G. M. & Rosado, J. A. Role of STIM2 in cell function and
779 physiopathology. *J Physiol* **595**, 3111-3128, doi:10.1113/jp273889 (2017).
780 72 Dietz, K. C., Polanco, J. J., Pol, S. U. & Sim, F. J. Targeting human oligodendrocyte progenitors
781 for myelin repair. *Experimental neurology* **283**, 489-500, doi:10.1016/j.expneurol.2016.03.017
782 (2016).
783 73 Kar, P., Bakowski, D., Di Capite, J., Nelson, C. & Parekh, A. B. Different agonists recruit
784 different stromal interaction molecule proteins to support cytoplasmic Ca2+ oscillations and
785 gene expression. *Proc Natl Acad Sci U S A* **109**, 6969-6974, doi:10.1073/pnas.1201204109
786 (2012).
787 74 Thiel, M., Lis, A. & Penner, R. STIM2 drives Ca2+ oscillations through store-operated Ca2+
788 entry caused by mild store depletion. *J Physiol* **591**, 1433-1445,
789 doi:10.1113/jphysiol.2012.245399 (2013).
790 75 Harriss, D. R., Marsh, K. A., Birmingham, A. T. & Hill, S. J. Expression of muscarinic M3-
791 receptors coupled to inositol phospholipid hydrolysis in human detrusor cultured smooth muscle
792 cells. *J Urol* **154**, 1241-1245 (1995).
793 76 Doherty, A. J., Palmer, M. J., Henley, J. M., Collingridge, G. L. & Jane, D. E. (RS)-2-chloro-5-
794 hydroxyphenylglycine (CHPG) activates mGlu5, but no mGlu1, receptors expressed in CHO
795 cells and potentiates NMDA responses in the hippocampus. *Neuropharmacology* **36**, 265-267,
796 doi:10.1016/s0028-3908(97)00001-4 (1997).

797 77 Pennington, L. D. *et al.* 4-Methoxy-N-[2-(trifluoromethyl)biphenyl-4-ylcarbamoyl]nicotinamide: A
798 Potent and Selective Agonist of S1P1. *ACS Med Chem Lett* **2**, 752-757, doi:10.1021/ml2001399
799 (2011).
800 78 Vassallo, R. R., Jr., Kieber-Emmons, T., Cichowski, K. & Brass, L. F. Structure-function
801 relationships in the activation of platelet thrombin receptors by receptor-derived peptides. *The*
802 *Journal of biological chemistry* **267**, 6081-6085 (1992).
803 79 Calleri, E. *et al.* Frontal affinity chromatography-mass spectrometry useful for characterization of
804 new ligands for GPR17 receptor. *J Med Chem* **53**, 3489-3501, doi:10.1021/jm901691y (2010).
805 80 Kawanabe, Y., Okamoto, Y., Enoki, T., Hashimoto, N. & Masaki, T. Ca(2+) channels activated
806 by endothelin-1 in CHO cells expressing endothelin-A or endothelin-B receptors. *American*
807 *journal of physiology. Cell physiology* **281**, C1676-1685, doi:10.1152/ajpcell.2001.281.5.C1676
808 (2001).
809 81 Chhatriwala, M. *et al.* Induction of novel agonist selectivity for the ADP-activated P2Y1 receptor
810 versus the ADP-activated P2Y12 and P2Y13 receptors by conformational constraint of an ADP
811 analog. *The Journal of pharmacology and experimental therapeutics* **311**, 1038-1043,
812 doi:10.1124/jpet.104.068650 (2004).
813 82 McGuire, J. J., Saifeddine, M., Triggle, C. R., Sun, K. & Hollenberg, M. D. 2-furoyl-LIGRLO-
814 amide: a potent and selective proteinase-activated receptor 2 agonist. *The Journal of*
815 *pharmacology and experimental therapeutics* **309**, 1124-1131, doi:10.1124/jpet.103.064584
816 (2004).
817 83 Tabarean, I. V. Functional pharmacology of H1 histamine receptors expressed in mouse
818 preoptic/anterior hypothalamic neurons. *Br J Pharmacol* **170**, 415-425, doi:10.1111/bph.12286
819 (2013).
820 84 Console-Bram, L., Brailoiu, E., Brailoiu, G. C., Sharir, H. & Abood, M. E. Activation of GPR18 by
821 cannabinoid compounds: a tale of biased agonism. *Br J Pharmacol* **171**, 3908-3917,
822 doi:10.1111/bph.12746 (2014).
823 85 Hinz, S., Lacher, S. K., Seibt, B. F. & Muller, C. E. BAY60-6583 acts as a partial agonist at
824 adenosine A2B receptors. *The Journal of pharmacology and experimental therapeutics* **349**,
825 427-436, doi:10.1124/jpet.113.210849 (2014).
826 86 Meis, S. *et al.* NF546 [4,4'-(carbonylbis(imino-3,1-phenylene-carbonylimino-3,1-(4-methyl-
827 phenylene)-car bonylimino))-bis(1,3-xylene-alpha,alpha'-diphosphonic acid) tetrasodium salt] is
828 a non-nucleotide P2Y11 agonist and stimulates release of interleukin-8 from human monocyte-
829 derived dendritic cells. *J Pharmacol Exp Ther* **332**, 238-247, doi:10.1124/jpet.109.157750
830 (2010).

831

832 **TABLES**

Primer	Sequence 5'-3'
WPRE	Forward: CGCTGCTTTAATGCCTTTGTAT
	Reverse: GGGCCACAACTCCTCATAAA
GAPDH	Forward: GTGAAGGTCGGAGTCAACGG
	Reverse: CCTGGAAGATGGTGATGGGA
STIM1	Forward: CCTCTCTTGACTCGCCATAATC
	Reverse: CTTGGAGTAACGGTTCTGGATATAG
STIM2	Forward: CAACACACACCACACTCCTT
	Reverse: GCCTCTTCCTCCTCTTCATTTC

833 **Table 1: qPCR primers.**

834

Gene Symbol	FPKM (hOPC; mOPCs)	Agonist/ Doses tested	Reported EC_{50}	% Responsive	Maximum amplitude	Duration (min)	% Oscillatory
CHRM3	16.3 ± 2.0; 0.27 ± 0.11	Oxo-M [25 μM]	2.5 μM [75]	67.6 ± 10.0	2.17 ± 0.06	6.1 ± 0.8	58.3 ± 20.5
CHRM1	4.0 ± 0.9; 2.06 ± 0.66						
GRM5	1.2 ± 0.004; 13.23 ± 3.63	CHPG [7.5 mM]	750μM [76]	46.9 ± 9.7	0.87 ± 0.03	6.7 ± 0.1	48.6 ± 4.1
S1PR1	3.1 ± 0.3; 34.32 ± 8.80	TC-G 1006 [350 nM]	35 nM [77]	27.8 ± 2.3	0.6 ± 0.02	2.3 ± 0.2	24.8 ± 14.1
F2R	26.7 ± 0.1; 23.54 ± 3.31	TRAP-6 [8.0 μM]	800 nM [78]	21.2 ± 13.3	1.0 ± 0.10	2.8 ± 0.5	38.9 ± 7.3
GPR17	3.6 ± 1.4; 440.98 ± 42.13	PF9 [400 pM]	36 pM [79]	19.3 ± 0.7	0.6 ± 0.01	2.3 ± 0.3	17 ± 10.3
EDNRB	17.3 ± 01; 292.72 ± 10.54	ET-1 [150 nM]	10 nM [80]	16.8 ± 4.3	1.03 ± 0.09	2.4 ± 0.3	28.8 ± 5.6
P2RY1	1.0 ± 0.2; 4.94 ± 1.46	MRS 2365 [12 nM]	1.2 nM [81]	14.6 ± 8.4	2.9 ± 0.20	9.3 ± 0.9	48.3 ± 0.3
HTR2B	0.8 ± 0.2; 0.12 ± 0.02	5-HT [100 μM]	* 10 μM [20]	13.0 ± 12.4	0.7 ± 0.08	2.1 ± 0.1	14.3 ± 14.3
F2RL1	1.3 ± 0.02; 0.10 ± 0.10	2-FLY [1.0 μM]	100 nM [82]	8.5 ± 1.3	1.6 ± 0.16	11.2 ± 0.2	63.7 ± 7.0
HRH1	0.4 ± 0.1; 5.01 ± 0.49	2-PED [560 μM]	56 μM [83]	7.4 ± 3.7	0.9 ± 0.06	3.1 ± 0.1	29.2 ± 4.2
GPR18	0.9 ± 0.4; 0.10 ± 0.10	NAGly [10 μM]	1 μM [84]	5.0 ± 3.9	1.3 ± 0.23	6.3 ± 3.5	21.8 ± 21.8
ADORA2B	0.6 ± 0.2; 8.79 ± 0.88	Bay [5.8 μM]	580 nM [85]	2.7 ± 2.7	0.4 ± 0.40	1.4 ± 1.4	12.5 ± 12.5
P2RY11	0.3 ± 0.1; –	NF 546 [5.0 μM]	500 nM [86]	1.1 ± 1.1	0.28 ± 0.28	0.9 ± 0.9	0.0 ± 0.0

Table 2: Human OPC-expressed $G\alpha_q$-coupled receptors differentially regulated oscillatory intracellular calcium fluctuations. RNA-seq data from human and mouse [46] was used to identify $G\alpha_q$-coupled receptors expressed by OPCs. FPKM values shown (mean ± SEM, n = 2 independent human fetal sample preparations). Ligands activating each receptor were identified to determine the calcium response characteristics in hOPCs. hOPCs were infected with GCaMP6s-expressing virus and exposed to various $G\alpha_q$-coupled receptor ligands at doses approximately 10-fold larger than reported EC_{50} values (or previously effective doses in rodent OPCs*). Calcium responses were recorded for at least 10 minutes and analyzed as described. The percentage of responding cells (at least 1 peak response ≥ 0.35 fold increase from baseline on normalized calcium trace following ligand addition), maximum response

845 amplitude (fold change from baseline), duration of response (minutes) and percentage of responding
846 cells displaying an oscillatory calcium response (cells with ≥ 2 identified peak responses) were
847 determined. While $G\alpha_q$-coupled LPA receptors LPAR1 and LPAR4 were detected in hOPCs, due to the
848 lack of specific ligands we did not test these receptors. Mean ± SEM of total % responsive cells from n=2-
849 3 independent human fetal sample culture preparations (Oxo-M, CHPG and ET-1 data: n=3 independent
850 fetal sample culture preparations; data for all additional ligands: n=2 individual fetal sample culture
851 preparations).
852
853 Abbreviations: **2-FLY**, 2-furoy-Leu-Ile-Gly-Arg-Leu-Orn-NH2; **2-PED**, 2-pyridylethylamide
854 dihydrochloride; **5-HT**, 5-hydroxytryptamine; **Bay**, Bay 60-6583 2-[[6-Amino-3 5-dicyano-4-[4-
855 cyclopropylmethoxy phenyl]-2-pyridinyl]thio]-acetamide; **CHPG**, 2-Chloro-5-hydroxyphenylglycine
856 sodium salt; **ET-1**, Endothelin-1; **MRS 2365**, [[(1R 2R 3S 4R 5S)-4-[6-Amino-2-(methylthio)-9H-purin-9-
857 yl]-2 3-dihydroxybicyclo[3.1.0]hex-1yl]methyl] diphosphoric acid mono ester trisodium salt; **NAGly**, N-
858 Arachidonoylglycine; **NF 546**, 4 4'-(Carbonylbis(imino-3 1-phenylene-carbonylimino-3 1-(4-methyl-
859 phenylene)carbonylimino))-bis(1 3-xylene-alpha alpha'-diphosphonic acid; **Oxo-M**, Oxotremorine
860 methiodide; **PF9**, 2-(Phenylethynyl)adenosine-5'-triphosphate tetrasodium salt; **TC-G**, 4-Methoxy-N-[[[2-
861 trifluoromethyl)[1 1'-biphenyl]-4-yl]amino]carbonyl]-3-pyridinecarboxamide; **TRAP-6**, Thrombin receptor
862 activating peptide 6.
863

FIGURE LEGENDS

Figure 1. $G\alpha_q$-receptor activation induces ER-Ca^{2+} responses and SOCE in primary human OPC. Primary fetal brain-derived PDGFαR$^+$ hOPCs were infected with intracellular Ca^{2+} reporter GCaMP6s expressing lentivirus. Time-lapse microscopy of GCaMP6s fluorescence following $G\alpha_q$-receptor agonist treatment was recorded and analyzed. **A,** pseudo-colored GCaMP6s fluorescence time-lapse images of oscillatory calcium transients following stimulation with Oxotremorine-M (Oxo-M) [2.5μM] (top) and CHPG [2.3mM] (bottom). **B**, shows corresponding normalized Ca^{2+} traces. Drug stimulation occurs at 0s (black arrow in B) and time following drug addition is indicated in each panel. Red and green dots indicated defined local maxima and minima, respectively. Gold dots indicated defined peaks. Images shown in A after drug addition correspond to calcium peaks (red) or post-peak minima (blue) and are indicated as arrows in B. Blue lines below traces indicate the calculated response duration. **C, D,** dose-response curves of the percentage of hOPCs responding to $G\alpha_q$ ligand treatment following treatment with either oxotremorine–M (Oxo-M) or CHPG (mean ± SEM, n=3 human fetal samples, >240 cells per biological replicate). **E, F,** dose-response curve for the log_{10}-transformed overall area under the curve (AUC) for $[Ca^{2+}]_i$ release per cell (mean ± SEM shown, n > 250 cells per dose, obtained from n=3 human fetal sample). EC_{50} for AUC was calculated by non-linear regression for each compound (variable slope, four parameters). **G**, to directly assess SOCE, GCaMP6s-expressing hOPCs were cultured in calcium-free conditions for 5-10 minutes prior to time-lapse microscopy. Following a 1-2m baseline, cells were treated with thapsigargin (Tg) or Oxo-M, followed by re-addition of calcium containing solution [1.2mM] to stimulate SOCE (green dashed lines) in the presence (middle and bottom traces) or absence (top trace) of SOCE antagonists. Calcium traces showing mean pixel intensity ± SEM (blue shading) of ≥ 44 cells from a single biological replicate. Timings for addition of Tg, Oxo-M and Ca^{2+}-containing solution are indicated by horizontal bars above each plot. **H**, quantification of SOCE was performed by analysis of AUC of calcium influx following calcium re-addition (mean ± SEM; Tg: n=2 human fetal sample preparations; OxoM: n=3 human fetal sample preparations). * $p<0.05$, RM one-way ANOVA with Holm-Sidak's post-hoc test. Scale: 25μm.

Figure 2. STIM1/2 calcium sensors are required for muscarinic-induced SOCE and $[Ca^{2+}]_i$ response in human OPCs. hOPCs were transfected with STIM1 and/or STIM2, or scrambled siRNA, cultured in mitogen-containing media, and RNA was extracted after 24-48 hours. For calcium imaging experiments, hOPCs were initially infected with GCaMP6s lentivirus and then transfected with STIM RNAi or scrambled control siRNA prior to time-lapse microscopy. RT-qPCR analysis of STIM1 (**A)** or STIM2 (**B**) mRNA expression relative to scrambled control transfected hOPCs following STIM1, STIM2 or STIM1/2 RNAi knockdown (STIM KD) (mean ± SEM, n=7-8 human samples). Control normalized mean

898 ± SEM, one-sample t-test, *p<0.05, **p<0.01, ****p<0.0001. **C**, representative pseudo-colored
899 fluorescence time-lapse images of peak Oxo-M-induced calcium responses in siRNA transfected hOPCs
900 cultured in calcium-free conditions. Images represent peak Oxo-M [25μM] induced ER-store depletion
901 (red text and arrows in **C** and **D** respectively) and SOCE following calcium re-addition (green text and
902 arrows in **C** and **D** respectively). **D**, calcium traces of Oxo-M induced calcium response following siRNA
903 transfection showing normalized mean pixel intensity ± SEM (blue shading) of n ≥ 30 cells per condition
904 from one representative biological replicate. Timings for addition of Oxo-M and Ca^{2+}-containing solution
905 are indicated by horizontal bars above plots. **E**, SOCE was measured as the total area under the curve
906 following calcium re-addition normalized to ER-release of control cells in the matched biological replicate.
907 STIM1/2 KD and pharmacological SOCE inhibition both resulted in a significant reduction in muscarinic-
908 induced SOCE relative to control hOPCs. Cells were analyzed across 1-2 imaging fields in a single well
909 per each condition and all responses were averaged per condition for each biological replicate. Data are
910 presented as mean ± SEM of averaged cell responses per each of four independent experiments, with
911 >140 total cells quantified per each condition, n=4 independent human fetal sample preparations. RM
912 one-way ANOVA with Holm-Sidak's post-hoc test, * p<0.05, ** p<0.01). **F–G**, the net effect of
913 pharmacological SOCE inhibition or STIM KD on Oxo-M-induced increased $[Ca^{2+}]_i$ was determined in
914 calcium-containing normal growth media by time-lapse microscopy. STIM1 KD or STIM2 KD hOPCs
915 displayed a reduction in Oxo-M-induced calcium responses as denoted by reduced average AUC (**F**) as
916 well as a reduction in oscillatory frequency relative to control hOPCs (**G**). Cells were analyzed across two
917 imaging fields in a single well per each condition and all responses were averaged per condition for each
918 biological replicate. Data represent log_{10}-transformed mean ± SEM of per cell responses from four
919 independent experiments (n=4 independent human fetal sample preparations), with >100 total cells
920 quantified per each condition. * p<0.05, ** p<0.01, *** p <0.001, ****p<0.0001, linear model with Tukey's
921 HSD posttest. Scale: 50 μm.
922
923 **Figure 3. Calcium sensor STIM2 regulates human OPC differentiation and is required for the anti-**
924 **differentiative effect of muscarinic agonists.** hOPCs were transfected with STIM1 and/or STIM2
925 siRNA, or control non-targeting siRNA, and 24 h later PDGF-AA and NT-3 were removed to induce
926 oligodendrocyte differentiation. **A**, representative images of immature $O4^+$ oligodendrocytes (green) in
927 the presence or absence of muscarinic agonist, Oxo-M [40μM]. **B**, quantification of the percentage of $O4^+$
928 oligodendrocyte differentiation among $DAPI^+$ cells (blue). Mean ± SEM shown (n=4 human fetal sample
929 culture). Differences in O4% were analyzed by RM three-way ANOVA using OxoM, STIM1, and STIM2
930 as factors and repeated measures across individual patient samples. Both Oxo-M and STIM2 siRNA
931 treatment resulted in a significant effect on $O4^+$ oligodendrocyte differentiation (OxoM: F (1, 3) = 14.31,

932 p = 0.032 and STIM2: F (1, 3) = 28.64, p = 0.0128). * p<0.05 and ** p<0.01 indicate pairwise Holm-Sidak
933 post-hoc tests. **C**, the percentage of dividing OPCs defined as KI-67$^+$/DAPI$^+$ cells following siRNA
934 transfection was determined in each group (n = 3 human samples). Neither STIM1/2 siRNA nor Oxo-M
935 treatment significantly influenced OPC proliferation (RM three-way ANOVA, main effects p > 0.05). Scale:
936 50 µm.
937
938 **Figure 4. OptoSTIM drives oscillatory calcium responses in hOPCs in the absence of $G\alpha_q$-coupled**
939 **signaling.** hOPCs were infected with OptoSTIM and jRCaMP1a lentiviruses to induce SOCE and
940 observe calcium responses simultaneously. Cells were cultured in a temperature/CO_2 controlled chamber
941 during time-lapse fluorescence microscopy. Blue light (488nm) excitation was used to induce SOCE at
942 distinct frequencies using 5 minute (3.33 mHz) or 30 minute (0.55 mHz) stimulation intervals respectively,
943 Blue light exposures were matched to ensure an equivalent amount of blue light stimulation across
944 conditions (330 and 2000 ms per stimulus, respectively). Changes in intracellular Ca^{2+} concentration
945 were assessed by jRCaMP1a fluorescence every 20 seconds. **A**, representative integrated calcium
946 response to OptoSTIM-induced SOCE in the absence of $G\alpha_q$-receptor activation. Images shown
947 represent total fluorescence across 2.5 hours of stimulation following a 30-minute baseline period. **B**,
948 jRCaMP1a traces of mean ± SEM (blue shading) normalized calcium responses to 0.55 mHz and 3.33
949 mHz frequencies over the course of 2.5 hours following a 30m baseline with no stimulation (n≥50 cells
950 from a single representative biological replicate). SOCE was robustly induced throughout the imaging
951 period and directly corresponded with the timing of blue light stimulation (vertical blue lines in middle and
952 lower traces). **C**, quantification of integrated calcium responses at different stimulation frequencies
953 measured for the duration of the stimulation period. Mean ± SEM of results from three independent
954 experiments (n=3 independent human fetal sample preparations) with >50 cells analyzed per condition/
955 replicate. * p<0.05, RM one-way ANOVA with Holm-Sidak's post-hoc test. Scale: 50 µm.
956
957 **Figure 5. SOCE is sufficient to block hOPC differentiation and promote hOPC mitosis.** Matched
958 cultures of primary hOPCs were infected with OptoSTIM lentivirus and imaged for 2-3 days in an on-
959 stage temperature/CO_2 controlled chamber. Bright field images were acquired every 5 minutes.
960 OptoSTIM-mediated SOCE was induced with intermittent 488nm excitation (5m or 30m interval for 330ms
961 and 2000ms duration, respectively). **A**, hOPC proliferation was quantified by counting mitotic events
962 (white arrowheads). **B**, the cumulative proportion of cells undergoing mitosis was quantified over 36 h
963 following the onset of blue light stimulation. **C,** proliferation rates were normalized to the matched
964 unstimulated condition. High frequency (3.33 mHz) OptoSTIM induction of SOCE resulted in a significant
965 increase in hOPC mitotic events compared to control unstimulated and low frequency (0.55 mHz)

966 stimulated hOPCs (n=4 independent human fetal sample culture preparations). **D**, the effect of
967 OptoSTIM-induced SOCE on hOPC differentiation was determined by O4 immunocytochemistry (red) at
968 48 hrs post-stimulation. OptoSTIM transduced cells were identified by GFP expression which was uniform
969 across experimental conditions (**E**). **F**, quantification of $O4^+$ oligodendrocyte differentiation following
970 OptoSTIM-induced SOCE (% $O4^+/GFP^+$). **G**, analysis of $O4^+$ morphological maturation. High frequency
971 (3.33 mHz) SOCE induced a significant reduction in $O4^+$ cells as well as a significant reduction in complex
972 branching morphology relative to control hOPCs. * $p<0.05$, Holm-Sidak's post-hoc test. Mean ± SEM
973 shown for each panel (n=4 independent human fetal samples). Scale: 25 µm.

Figure 1

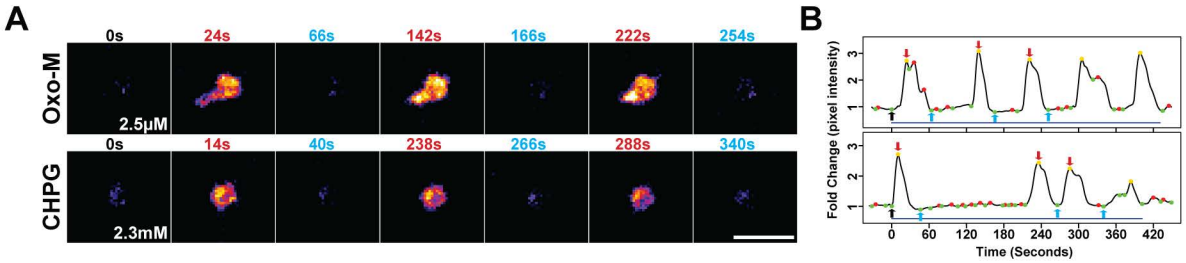
A
0s
24s
66s
142s
166s
222s
254s
Oxo-M
2.5μM
0s
14s
40s
238s
266s
288s
340s
CHPG
2.3mM
B
Fold Change (pixel intensity)
Time (Seconds)

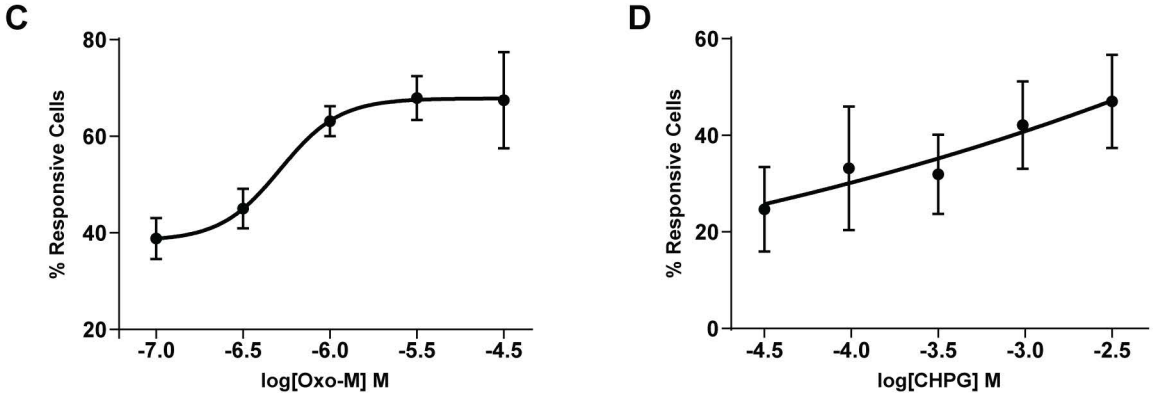
C
% Responsive Cells
log[Oxo-M] M
D
% Responsive Cells
log[CHPG] M

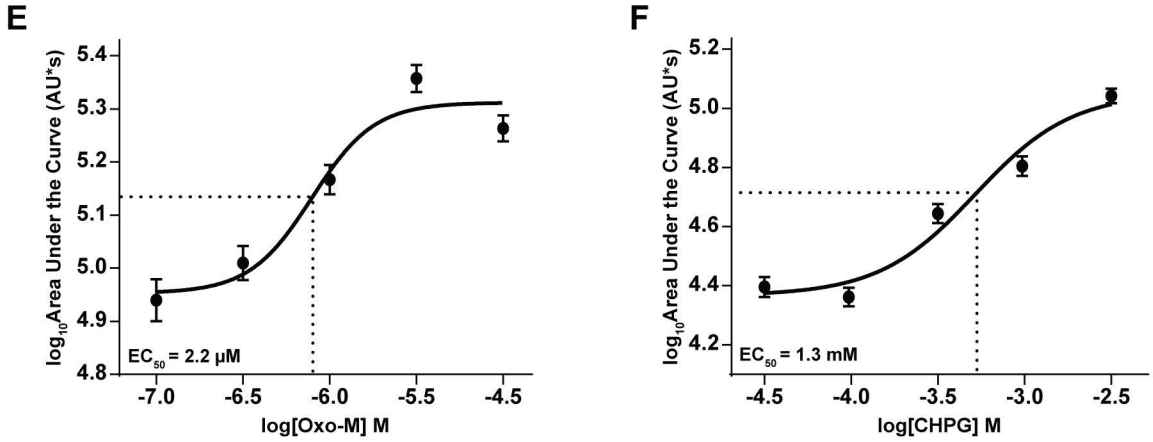
E
log10 Area Under the Curve (AU*s)
EC50 = 2.2 μM
log[Oxo-M] M
F
log10 Area Under the Curve (AU*s)
EC50 = 1.3 mM
log[CHPG] M

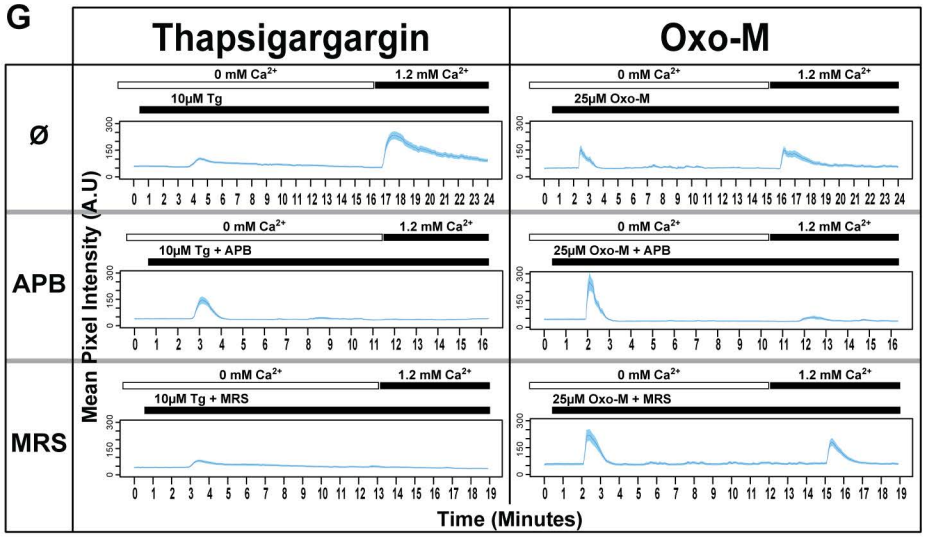
G
Thapsigargargin
Oxo-M
Ø
APB
MRS
0 mM Ca2+
1.2 mM Ca2+
10μM Tg
25μM Oxo-M
10μM Tg + APB
25μM Oxo-M + APB
10μM Tg + MRS
25μM Oxo-M + MRS
Mean Pixel Intensity (A.U)
Time (Minutes)

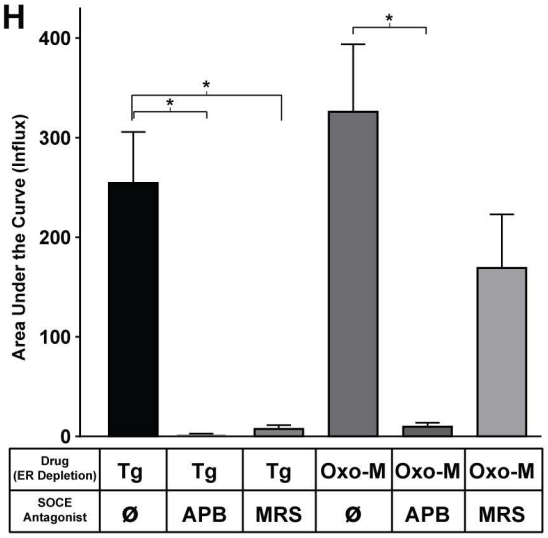
H
Area Under the Curve (Influx)
Drug (ER Depletion)
Tg
Tg
Tg
Oxo-M
Oxo-M
Oxo-M
SOCE Antagonist
Ø
APB
MRS
Ø
APB
MRS

Figure 2

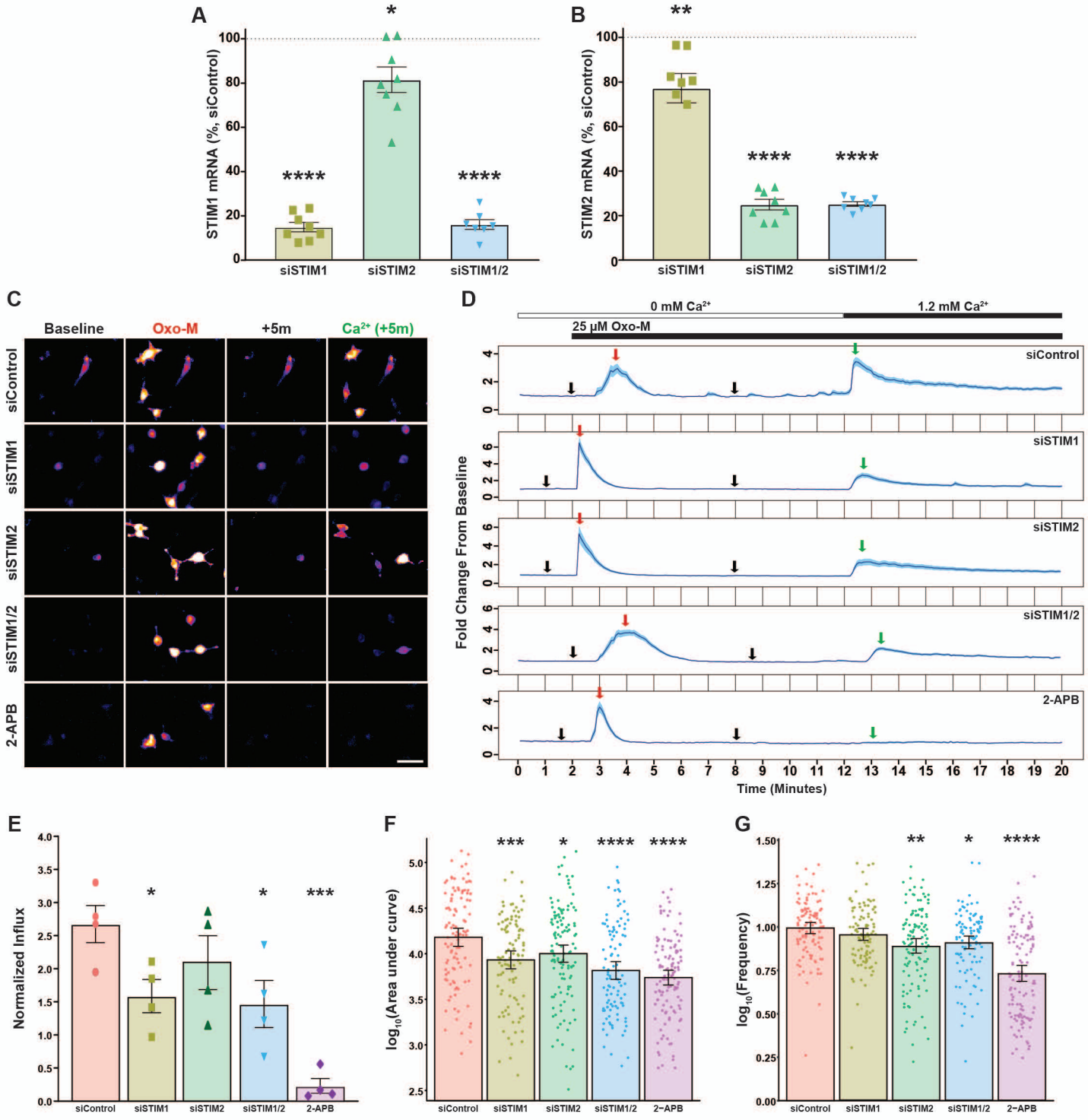
A
STIM1 mRNA (%, siControl)
siSTIM1
siSTIM2
siSTIM1/2
B
STIM2 mRNA (%, siControl)
C
Baseline
Oxo-M
+5m
Ca2+ (+5m)
siControl
siSTIM1
siSTIM2
siSTIM1/2
2-APB
D
0 mM Ca2+
1.2 mM Ca2+
25 μM Oxo-M
Fold Change From Baseline
Time (Minutes)
E
Normalized Influx
F
log10(Area under curve)
G
log10(Frequency)

Figure 3

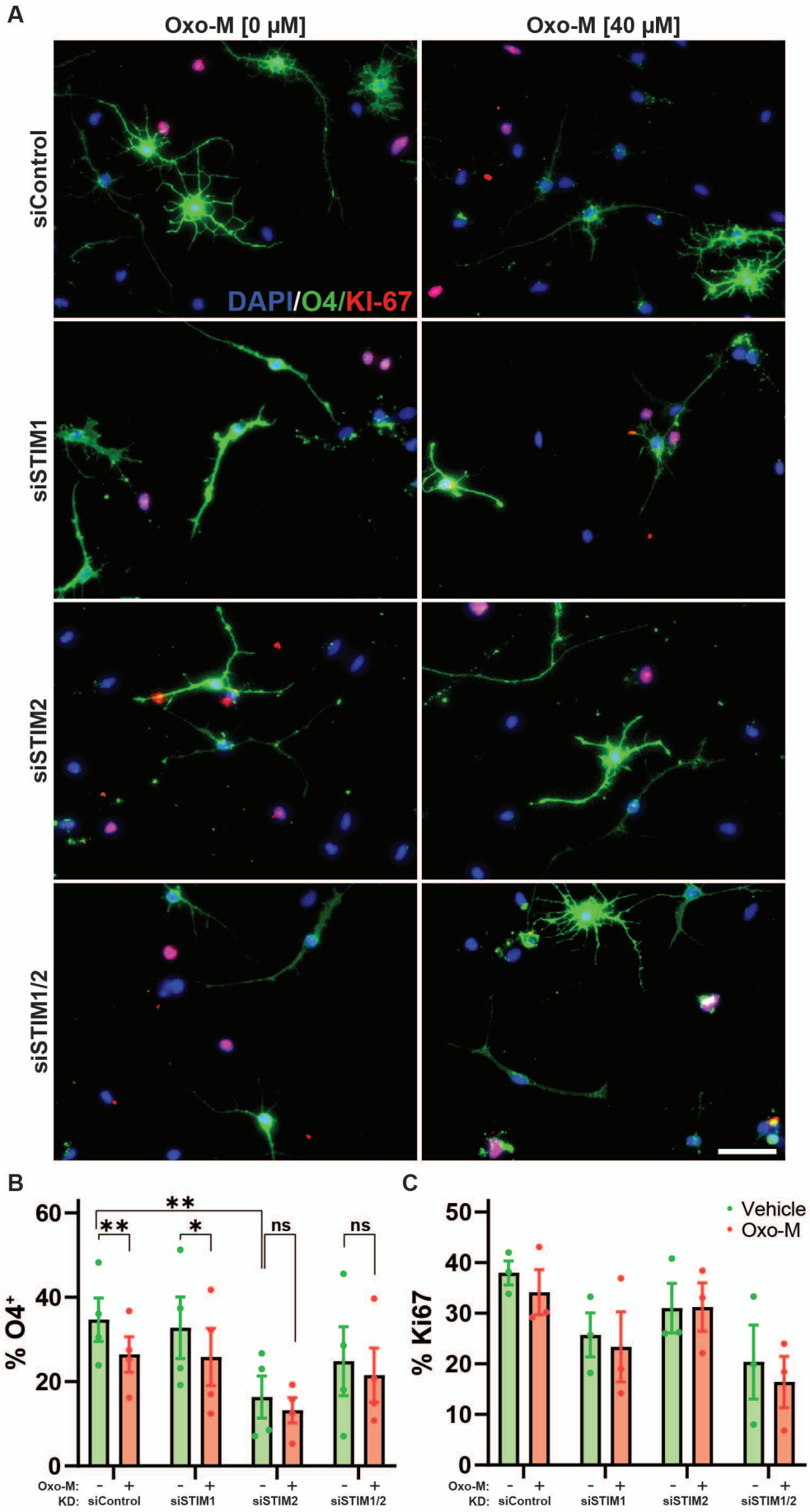
A
Oxo-M [0 μM]
Oxo-M [40 μM]
siControl
siSTIM1
siSTIM2
siSTIM1/2
DAPI/O4/KI-67
B
% O4+
60
40
20
0
**
**
*
ns
ns
Oxo-M: - + - + - + - +
KD: siControl siSTIM1 siSTIM2 siSTIM1/2
C
% Ki67
50
40
30
20
10
0
Vehicle
Oxo-M
Oxo-M: - + - + - + - +
KD: siControl siSTIM1 siSTIM2 siSTIM1/2

Figure 4

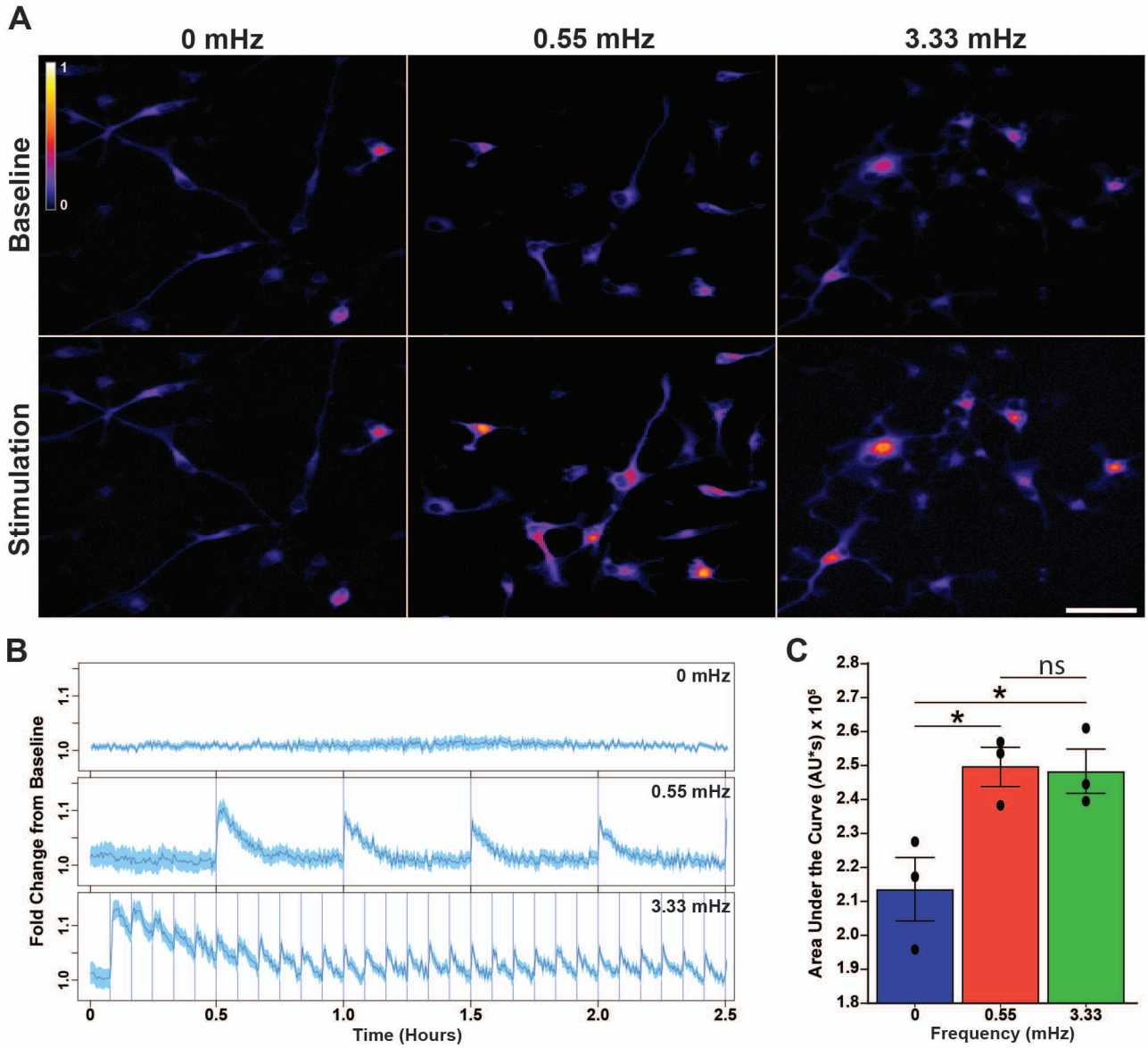
A
0 mHz
0.55 mHz
3.33 mHz
Baseline
Stimulation
1
0
B
0 mHz
0.55 mHz
3.33 mHz
Fold Change from Baseline
1.1
1.0
0
0.5
1.0
1.5
2.0
2.5
Time (Hours)
C
ns
*
*
Area Under the Curve (AU*s) x 10^5
2.8
2.7
2.6
2.5
2.4
2.3
2.2
2.1
2.0
1.9
1.8
0
0.55
3.33
Frequency (mHz)

Figure 5

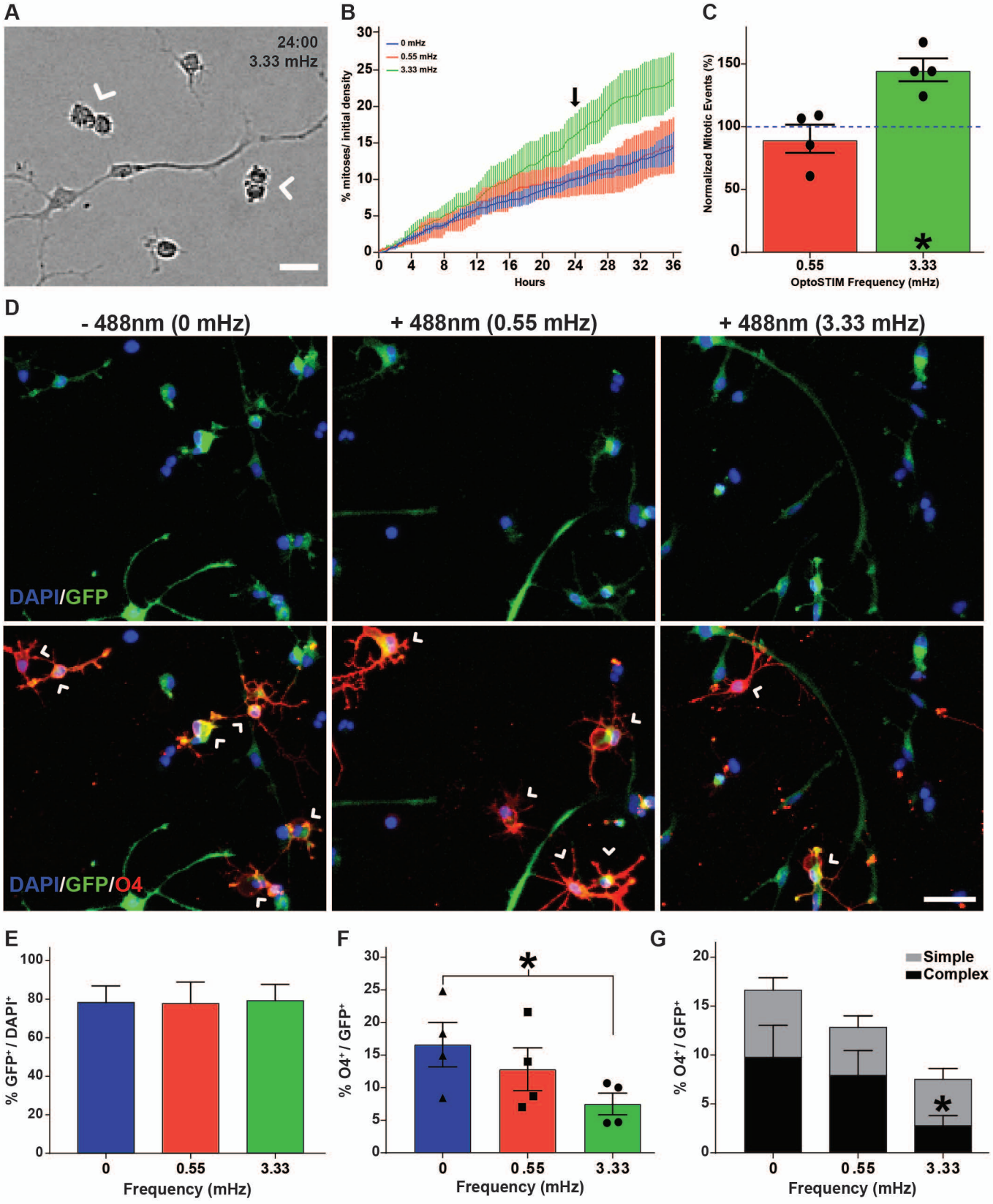
A
24:00
3.33 mHz
B
0 mHz
0.55 mHz
3.33 mHz
% mitoses/ initial density
Hours
C
Normalized Mitotic Events (%)
0.55
3.33
OptoSTIM Frequency (mHz)
D
- 488nm (0 mHz)
+ 488nm (0.55 mHz)
+ 488nm (3.33 mHz)
DAPI/GFP
DAPI/GFP/O4
E
% GFP+ / DAPI+
Frequency (mHz)
F
% O4+ / GFP+
Frequency (mHz)
G
Simple
Complex
% O4+ / GFP+
Frequency (mHz)